Influence of evaporation and seepage on the convergence of a ventilated cavity

Pierre Gerard,[1] Robert Charlier,[1] René Chambon,[2] and Frédéric Collin[1]

Received 6 September 2007; revised 29 February 2008; accepted 27 March 2008; published 19 July 2008.

[1] In the design of nuclear waste disposals, an important topic concerns the development of an excavated damage zone, where permeability increases. A correct numerical prediction of the coupled processes occurring during excavation is therefore needed. In this paper, a nonclassical hydraulic boundary condition is described. It mixes two modes of water exchanges in partial saturation: seepage and evaporation flows. Seepage flow avoids unphysical water inflow into the rock mass, which might be obtained with usual boundary condition in dilatant geomaterial. Evaporation flows enable the thermodynamical equilibrium between air relative humidity in the cavity and in the rock mass. The numerical modeling of a cavity excavation in dilatant geomaterial is carried out. The results show the influence of the hydraulic boundary condition on the convergence of the cavity. Depending on the value of the transfer coefficient, the proposed numerical model can recover the results obtained with an imposed atmospheric pressure or suction at the cavity wall. The determination of the mass transfer coefficient is thus needed and can be achieved through drying experiments or can be estimated thanks to in situ measurements.

Citation: Gerard, P., R. Charlier, R. Chambon, and F. Collin (2008), Influence of evaporation and seepage on the convergence of a ventilated cavity, *Water Resour. Res.*, *44*, W00C02, doi:10.1029/2007WR006500.

1. Introduction

[2] Deep geological layers are being considered potential host rocks for the high-level radioactivity waste disposals. Some underground research facilities (URF) have been constructed in Europe [*Neerdael and Boyazis*, 1997; *Delay et al.*, 2007] and in the USA [*Rutqvist et al.*, 2005], in order to study the feasibility of such network of galleries. The main purpose of underground waste disposals is the preservation of the human activities from the radioactivity effects. The potential geological host layers have a common property: their permeability is very low. All the altering processes of this natural barrier are thus crucial issues. An important topic concerns the development of an excavated damage zone (named EDZ) around the galleries. This EDZ increases the permeability of the host formation and consequently the radionuclides migration as well. A correct numerical prediction of the coupled processes occurring during the excavation is therefore needed. For this purpose, a constitutive model of the mechanical behavior is necessary. The present paper will not focus on the constitutive law but will show the significant influence of both the constitutive law and the hydraulic boundary condition at the cavity wall on the response of the dilatant geomaterial with a low permeability. Indeed the usual boundary condition (for the flow problem) during excavation is a progressive decrease of the pore water pressure down to the atmospheric pressure. On one hand, such boundary condition could predict an unphysical pore water pressure distribution (see section 6). On the other hand, the relative humidity in the cavity is usually controlled thanks to a ventilation system. This could be modeled by a decrease of the pore water pressure at the cavity wall down to the corresponding suction at the end of the excavation [*Hoxha et al.*, 2004]. This boundary condition relies on the assumption of a quasi-instantaneous equilibrium between the air relative humidity and the pore water pressure of the cavity wall. This assumption could be too optimistic. This highlights the need of a more detailed expression of the water exchanges between humid air in the cavity and the rock mass. Two modes of exchange can occur: seepage flow and vapor flow [*Ghezzehei et al.*, 2004]. The seepage flows are liquid flows that are introduced for solving free surface seepage problem. Following the ideas of *Brezis et al.* [1978] and *Bardet and Tobita* [2002], seepage condition is imposed as a Signorini's type condition on the water pressure. Vapor exchanges occur when the relative humidities in the cavity air and rock mass are different. Several formulations of the vapor flows can be found in the literature, which usually assume that the flow is proportional to the difference of relative humidity [*Anagnostou*, 1995], vapor pressure [*Zhongxuan et al.*, 2004], the vapor potential [*Kowalski*, 1997] or the vapor density [*Ben Nasrallah and Pere*, 1988]. The proportionality coefficient (or mass transfer coefficient) is usually determined through experiments as a complex function of different parameters such as the degree of saturation, the porosity or the wind velocity in the cavity [*Dracos*, 1980; *Anagnostou*, 1995; *Zhongxuan et al.*, 2004].

[3] In this paper, a quasi-static formulation of the balance equations of a porous medium is first recalled in section 2.

[1] Architecture, Géologie, Environnement et Constructions, Université de Liège, Liège, Belgium.
[2] Laboratoire 3S, UJF, INPG, CNRS, Grenoble, France.

0043-1397/08/2007WR006500$09.00

The expression of the water exchange flows occurring at the cavity wall is described in section 3. In order to solve numerically the field equations, a linear auxiliary problem is defined following the approach of *Borja and Alarcon* [1995] (section 4) and the field of unknowns is obtained through a Newton-Raphson scheme. In section 5, the linear auxiliary problem is discretized using the finite element methodology [*Zienkiewicz and Taylor*, 2000]. Large strain isoparametric coupled finite element and boundary finite element formulations are proposed. The water exchange flows will be discretized by a special finite element, which aims modeling the hydraulic boundary condition. Finally, an example of the influence of the hydraulic boundary condition will be presented for the excavation and the ventilation of a deep cylindrical cavity (section 6).

2. Balance Equations of a Porous Medium

[4] In the numerical study, the geomaterials of the geological layer are porous media generally considered as the superposition of several continua [*Coussy*, 1995]: the solid skeleton (grains assembly) and the fluid phases (water, air, oil...). On the basis of averaging theories [*Hassanizadeh and Gray*, 1979a, 1979b], *Lewis and Schrefler* [2000] proposed the governing equations for the full dynamic behavior of a partially saturated porous medium. Hereafter these equations are restricted for quasi-static problem in unsaturated conditions, under Richard's assumptions (constant air pressure). This assumption may be irrelevant in the particular case of low and ultralow permeable porous media. For this study, isothermal condition and incompressible solid grains are assumed. The unknowns of the mechanical and the flow problems are respectively the displacements u_i and the pore water pressure p_w (possibly negative in unsaturated case). In the following developments, the balance equations are written in the current solid configuration denoted Ω^t (updated Lagrangian formulation).

2.1. Balance of Momentum

[5] In the mixture balance of momentum equation, the interaction forces between fluid phases and grain skeleton cancels. In a weak form (virtual work principle), this equation reads for any kinematically admissible virtual displacement field u_i^*:

$$\int_{\Omega^t} \sigma_{ij}^t \varepsilon_{ij}^* d\Omega^t = \int_{\Omega^t} \left(\rho_s(1-\phi^t) + S_{r,w}^t \rho_w^t \phi^t\right) g_i u_i^* d\Omega^t + \int_{\Gamma_\sigma^t} \overline{t}_i^t u_i^* d\Gamma^t \tag{1}$$

where $\varepsilon_{ij}^* = \frac{1}{2}((\partial u_i^*/\partial x_j^t) + (\partial u_j^*/\partial x_i^t))$ is the kinematically admissible virtual strain field, ϕ^t is the porosity defined as $\phi^t = \Omega^{v,t}/\Omega^t$ where Ω^t is the current volume of a given mass of skeleton and $\Omega^{v,t}$ the corresponding porous volume, ρ_s is the solid grain density, $S_{r,w}^t$ is the water relative saturation, ρ_w^t is the water density, g_i is the gravity acceleration and Γ_σ^t is the part of the boundary where tractions $\overline{t}_i^t$ are known.

[6] The total stress σ_{ij}^t is defined as a function of the kinematics. Here we assume first that the Bishop's definition of effective stress holds [*Nuth and Laloui*, 2008]:

$$\sigma_{ij}^t = \sigma_{ij}'^t - S_{r,w}^t p_w^t \delta_{ij} \tag{2}$$

with $\sigma_{ij}'^t$ the effective stress, p_w^t the pore water pressure and δ_{ij} the Kronecker symbol.

2.2. Mass Balance Equations

[7] The water mass balance equation reads in a weak form:

$$\int_{\Omega^t} \left(\dot{M}^t p_w^* - m_i^t \frac{\partial p_w^*}{\partial x_i^t}\right) d\Omega^t = \int_{\Omega^t} Q^t p_w^* d\Omega^t - \int_{\Gamma_q^t} \overline{q}^t p_w^* d\Gamma^t \tag{3}$$

where p_w^* is the virtual pore water pressure field, Q^t is a sink term and Γ_q^t is the part of the boundary where the input water mass per unit area $\overline{q}^t$ is prescribed. M^t and m_i^t are respectively the mass of the water inside the current configuration of the skeleton Ω^t and the mass flow. They are defined hereafter respectively in equation (6) and equation (4).

[8] Water mass balance equation (equation (3)) has to hold for any time t, the virtual quantities in this equation being dependant on the history of boundary conditions and on time t.

[9] The mass flow m_i^t is defined as follows:

$$m_i^t = -\rho_w^t \frac{\kappa k_{r,w}^t}{\mu_w} \left(\frac{\partial p_w^t}{\partial x_i^t} + \rho_w^t g_i\right) \tag{4}$$

where κ is the intrinsic permeability, $k_{r,w}^t$ is water relative permeability and μ_w is the water dynamic viscosity.

[10] The compressible fluid is assumed to respect the following relationship [*Lewis and Schrefler*, 2000]. This predicts an increase of water density as a function of the pore water pressure, defining χ_w as the water bulk modulus:

$$\dot{\rho}_w^t = \frac{\rho_w^t}{\chi_w} \dot{p}_w^t \tag{5}$$

If the grains are assumed to be incompressible (which means ρ_s is constant), the time derivative of the water mass is obtained directly by using equation (5) and mass balance equation for the solid phase. This yields for a unit mixture volume:

$$\dot{M}^t = \rho_w^t \left[\frac{\dot{p}^t}{\chi_w} S_{r,w}^t \phi^t + \dot{S}_{r,w}^t \phi^t + S_{r,w}^t \frac{\dot{\Omega}^t}{\Omega^t}\right] \tag{6}$$

3. Water and Vapor Exchanges at the Cavity Wall

[11] During the excavation processes, the pore water pressure at the cavity wall is decreasing. After excavation, we may consider for long-term predictions that a thermodynamical equilibrium is reached between the cavity air and the rock mass. The wall moisture tends to be in equilibrium with the air humidity in the tunnel thanks to liquid water and vapor exchanges occurring at the boundary between cavity and rock mass. Because of plastic dilatancy of the material, the numerical hydromechanical modeling with classical boundary conditions of the flow problem provides totally unphysical results as an injection of a huge amount of water in the medium during excavation. Nonclassical boundary condition such as seepage or vapor exchanges has to be considered to correctly model the hydromechanical processes.

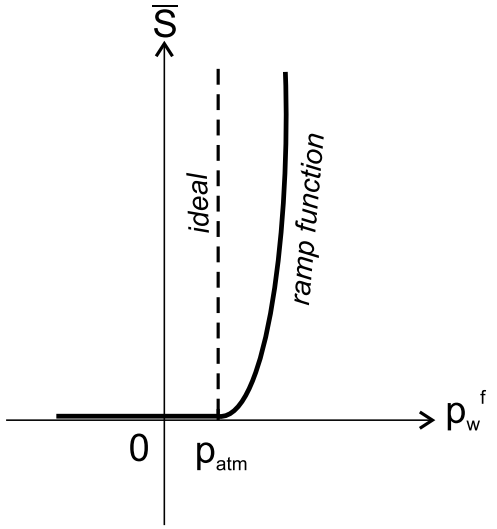

Figure 1. Seepage boundary condition.

[12] Seepage flows occur only when the pore water pressure at the cavity wall is larger than the cavity air pressure. The seepage condition can be expressed as a unilateral flow condition (Signorini's boundary condition) in order to avoid water inflow into the rock mass (Figure 1). For computational purpose, this condition is introduced in a finite element code using a ramp function [*Bardet and Tobita*, 2002; *Zheng et al.*, 2008] (Figure 1). The ramp function gives the expression of the seepage liquid flow $\overline{S}$:

$$\begin{cases} \overline{S} = \beta.\left(p_w^f - p_{atm}\right)^2 & \text{if } p_w^f \geq p_w^{cav} \text{ and } p_w^f \geq p_{atm} \\ \overline{S} = 0 & \text{if } p_w^f < p_w^{cav} \text{or } p_w^f < p_{atm} \end{cases} \quad (7)$$

with p_w^f the pore water pressure in the rock mass formation, p_w^{cav} the water pressure corresponding to the relative humidity in the cavity (using equation (10)), p_{atm} the atmospheric pressure and β a seepage transfer coefficient. This transfer coefficient should be as high as possible compare to the permeability of the medium, in order to respect the seepage condition.

[13] Vapor exchanges occur when a difference between relative humidities in cavity air and rock mass exists. In the following, the conceptual model for the vapor exchanges relies on the existence of a locally uniform distribution of vapor concentration on the cavity porous surface [*Ghezzehei et al.*, 2004]. The exchange takes place between the cavity wall and the cavity atmosphere through a boundary layer, which thickness controls the vapor transfer.

[14] Vapor inflows or outflows are physically possible. Several formulations of these fluxes can be found in the literature. Each of them is using a mass transfer coefficient which can be expressed as a function of the degree of saturation, the porosity or the air velocity in the cavity [*Dracos*, 1980; *Anagnostou*, 1995; *Zhongxuan et al.*, 2004]. To obtain the evaporation flow, this mass transfer coefficient can be multiplied by the difference of relative humidity [*Anagnostou*, 1995], vapor pressure [*Zhongxuan et al.*, 2004] or vapor potential [*Kowalski*, 1997] between cavity air and the geological formation. As proposed by *Ben Nasrallah and Pere* [1988], we choose to express vapor exchanges as the difference of vapor density between the tunnel atmosphere and rock mass:

$$\overline{E} = \alpha\left(\rho_v^f - \rho_v^{cav}\right) \quad (8)$$

with ρ_v^f and ρ_v^{cav} vapor density respectively in the formation and in the cavity and α a vapor mass transfer coefficient.

[15] In isothermal conditions, the different evaporation flow expressions give identical results, if the value of mass transfer coefficient is modified upon the chosen formulation. In anisothermal conditions, a new nonlinearity is introduced, because vapor mass transfer coefficient depends itself on temperature. Experimentations at different temperatures are thus necessary to determine the thermal sensitivity of this coefficient.

[16] The vapor density ρ_v is given by the following thermodynamic relationship:

$$\rho_v = h\rho_{v,0} \quad (9)$$

where h is the relative humidity and $\rho_{v,0}$ the saturated vapor density.

[17] Relative humidity in porous medium is related to the capillary pressure p_c by the Kelvin's law:

$$h = \exp\left(-\frac{p_c M_v}{R\rho_w T}\right) \quad (10)$$

with p_c the capillary pressure ($p_c = p_g - p_w$), M_v vapor molar mass (0.018 kg mol^{-1}), R the molar gas constant (8.134 J mol^{-1} K^{-1}), T the absolute temperature (°K) and ρ_w the water density.

[18] Saturated vapor density is obtained by ideal gas law:

$$\rho_{v,0} = \frac{p_{v,0} M_v}{R.T} \quad (11)$$

where $p_{v,0}$ is the saturated vapor pressure given by the experimental expression following [*Collin*, 2003]:

$$p_{v,0} = a\exp(-b/T) \quad (12)$$

with a = 112659 MPa and b = 5192.74 for temperatures 26
included between 273°K and 373°K.

[19] Other possibility to obtain the saturated vapor density consists of defining an empirical relationship on the basis of experimental results. For example, for temperatures included between 293 and 331°K, *Ewen and Thomas* [1989] have proposed the following relationship on the basis of data from *Mayhew and Rogers* [1976]:

$$\frac{1}{\rho_{v,0}} = 194.4\exp\left[-0.06374(T-273) + 0.1634\times10^{-3}(T-273)^2\right] \quad (13)$$

[20] On the basis of previous expressions, the total flow $\overline{q}$ between cavity air and the geological formation is simply expressed as the sum of the seepage flow and vapor exchange flow:

$$\overline{q} = \overline{S} + \overline{E} \quad (14)$$

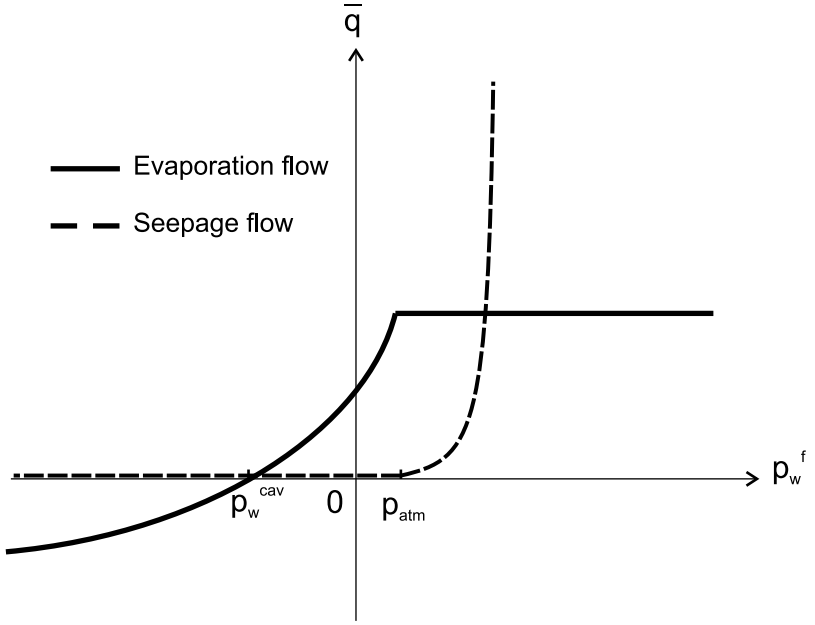

Figure 2. Evaporation and seepage flows.

[21] Because of permanent air ventilation of the cavities, we can consider that air relative humidity and vapor density in the tunnel are constant. Evaporation and seepage flows evolve thus according to the value of water pressure p_w^f at the cavity wall (Figure 2).

[22] Initially, if rock mass humidity is higher than cavity air humidity ($p_w^f \geq p_{atm} > p_w^{cav}$), vapor exchanges take place from the geological formation to the cavity. Evaporation flows remain constant as long as rock mass is totally saturated ($p_w^f > p_{atm}$). When pore water pressure is lower than atmospheric pressure, the geological formation is desaturated and vapor exchanges decrease until the equilibrium between porous medium and ambient atmosphere is obtained. Seepage flows exist only if pore water pressure at the cavity wall is higher than pressure in the cavity atmosphere.

[23] If rock mass humidity is lower than cavity air humidity ($p_w^f < p_{atm}$ and $p_w^f < p_w^{cav}$), condensation flows take place from the tunnel atmosphere into the formation in order to resaturate the rock mass. The saturation increases progressively to reach the tunnel relative humidity level. On the other hand, no seepage flow occurs.

4. Linearization of the Field Equations

[24] For a given boundary value problem at time τ, the equilibrium is not a priori met and some residuals appears in the expression of the field equations (equations (1) and (3)), which can be rewritten as follows:

$$\int_{\Omega^\tau} \sigma_{ij}^\tau \frac{\partial u_i^*}{\partial x_j^\tau} d\Omega^\tau - \int_{\Omega^\tau} \left(\rho_s(1-\phi^\tau) + S_{r,w}^\tau \rho_w^\tau \phi^\tau\right) g_i u_i^* d\Omega^\tau - \int_{\Gamma_\sigma^\tau} \overline{t}_i^\tau u_i^* d\Gamma^\tau = R^\tau \tag{15}$$

$$\int_{\Omega^\tau} \left(\dot{M}^\tau p_w^* - m_i^\tau \frac{\partial p_w^*}{\partial x_i^\tau}\right) d\Omega^\tau - \int_{\Omega^\tau} Q^\tau p_w^* d\Omega^\tau + \int_{\Gamma_q^\tau} \overline{q}^\tau p_w^* d\Gamma^\tau = W^\tau \tag{16}$$

with R^τ and W^τ respectively the mechanical and the flow residuals.

[25] A Newton-Raphson scheme is proposed to find a new solution of displacements and pressures field, for which equilibrium is met. The idea is to define a linear auxiliary problem deriving from the continuum one (instead of the discretized one as it is more usually done) similar to the work of *Borja and Alarcon* [1995]. This approach gives the same results as standard FEM procedure but make the linearization easier, especially for coupled problem in large strain formulation.

[26] If we assume known the configuration of Ω^t (x_i^t and p_w^t) at time t in equilibrium with boundary conditions, the objective is to find the new configuration in equilibrium at the end of the time step ($\tau = t + \Delta t$). A first guess of a new configuration $\Omega^{\tau 1}$ ($x_i^{\tau 1}$ and $p_w^{\tau 1}$) is realized, for which the equilibrium is not met. Mechanical and flow residuals flow $R^{\tau 1}$ and $W^{\tau 1}$ exist, as shown in equations (15) and (16). The aim is to find a new configuration $\Omega^{\tau 2}$, close to $\Omega^{\tau 1}$, for which the residuals $R^{\tau 2}$ and $W^{\tau 2}$ vanish. In order to get the linear auxiliary problem, the field equations corresponding to $\Omega^{\tau 2}$ are rewritten in configuration $\Omega^{\tau 1}$ (using the Jacobian transformation) and the resulting equations are subtracted from the corresponding initial equations written in configuration $\Omega^{\tau 1}$.

[27] In this paper, linearization of balance of momentum equation (equation (15)) is not developed. We refer to developments in the work of *Collin et al.* [2006] and the results are presented hereafter. Concerning linearization of mass balance equation for the water (equation (16)), *Collin et al.* [2006] present developments when second terms of mass balance equation do not vary according to the configuration $\Omega^{\tau 1}$ or $\Omega^{\tau 2}$, because $\overline{q}^t$ and Q are assumed displacement and hydraulic field independent. In our formulation, water mass per unit area $\overline{q}^t$ is defined in equation (14) and is pore water pressure dependent. Second terms of mass balance equation for the water are then modified with configuration variations. The subtraction of field equation

corresponding to $\Omega^{\tau 2}$ is rewritten in configuration $\Omega^{\tau 1}$ (using the Jacobian transformation) with corresponding equation in configuration $\Omega^{\tau 1}$ becomes

$$\int_{\Omega^{\tau 1}} p_w^* \begin{pmatrix} d\rho_w^{\tau 1} S_{r,w}^{\tau 1} \dfrac{\phi^{\tau 1}}{\chi_w} \dot{p}_w^{\tau 1} + \rho_w^{\tau 1} S_{r,w}^{\tau 1} \dfrac{d\phi^{\tau 1}}{\chi_w} \dot{p}_w^{\tau 1} + \rho_w^{\tau 1} S_{r,w}^{\tau 1} \dfrac{\phi^{\tau 1}}{\chi_w} \dfrac{dp_w^{\tau 1}}{\Delta t} + \rho_w^{\tau 1} dS_{r,w}^{\tau 1} \dfrac{\phi^{\tau 1}}{\chi_w} \dot{p}_w^{\tau 1} \\ + \; d\rho_w^{\tau 1} \dot{S}_{r,w}^{\tau 1} \phi^{\tau 1} + \rho_w^{\tau 1} \dfrac{dS_{r,w}^{\tau 1}}{\Delta t} \phi^{\tau 1} + \rho_w^{\tau 1} \dot{S}_{r,w}^{\tau 1} d\phi^{\tau 1} + d\rho_w^{\tau 1} S_{r,w}^{\tau 1} \dfrac{\dot{\Omega}^{\tau 1}}{\Omega^{\tau 1}} \\ + \; \rho_w^{\tau 1} dS_{r,w}^{\tau 1} \dfrac{\dot{\Omega}^{\tau 1}}{\Omega^{\tau 1}} + \rho_w^{\tau 1} S_{r,w}^{\tau 1} \left(\dfrac{\partial du_m^{\tau 1}}{\partial x_m^{\tau 1}} \dfrac{1}{\Delta t} - \dfrac{\dot{\Omega}^{\tau 1}}{\Omega^{\tau 1}} \dfrac{\partial du_m^{\tau 1}}{\partial x_m^{\tau 1}} \right) + \dot{M}^{\tau 1} \dfrac{\partial du_m^{\tau 1}}{\partial x_m^{\tau 1}} \end{pmatrix} d\Omega^{\tau 1}$$

$$- \int_{\Omega^{\tau 1}} \frac{\partial p_w^*}{\partial x_l^{\tau 1}} \begin{pmatrix} -d\rho_w^{\tau 1} \dfrac{\kappa k_{r,w}^{\tau 1}}{\mu_w} \left(\dfrac{\partial p_w^{\tau 1}}{\partial x_l^{\tau 1}} + \rho_w^{\tau 1} g_l \right) - \rho_w^{\tau 1} \dfrac{\kappa k_{r,w}^{\tau 1}}{\mu_w} \left(\dfrac{\partial dp_w^{\tau 1}}{\partial x_l^{\tau 1}} + d\rho_w^{\tau 1} g_l \right) \\ -\rho_w^{\tau 1} \dfrac{\kappa}{\mu_w} dk_{r,w}^{\tau 1} \left(\dfrac{\partial p_w^{\tau 1}}{\partial x_l^{\tau 1}} + \rho_w^{\tau 1} g_l \right) + \rho_w^{\tau 1} \dfrac{\kappa k_{r,w}^{\tau 1}}{\mu_w} \dfrac{\partial du_j^{\tau 1}}{\partial x_l^{\tau 1}} \dfrac{\partial p_w^{\tau 1}}{\partial x_j^{\tau 1}} \\ -m_j^{\tau 1} \dfrac{\partial du_l^{\tau 1}}{\partial x_j^{\tau 1}} + m_l^{\tau 1} \dfrac{\partial du_m^{\tau 1}}{\partial x_m^{\tau 1}} \end{pmatrix} d\Omega^{\tau 1}$$

$$= \int_{\Gamma_q^{\tau 1}} p_w^* \left(d\overline{q}^{\tau 1} + \overline{q}^{\tau 1} \frac{\partial du_m^{\tau 1}}{\partial x_m^{\tau 1}} \right) d\Gamma^{\tau 1} - W^{\tau 1} \tag{25}$$

$$\int_{\Omega^{\tau 1}} \left[\left(\dot{M}^{\tau 2} \mathbf{det} F - \dot{M}^{\tau 1} \right) p_w^* - \frac{\partial p_w^*}{\partial x_l^{\tau 1}} \left(m_i^{\tau 2} \frac{\partial x_l^{\tau 1}}{\partial x_i^{\tau 2}} \mathbf{det} F - m_l^{\tau 1} \right) \right] d\Omega^{\tau 1} = \int_{\Gamma_q^{\tau 1}} \left(\overline{q}^{\tau 2} \mathbf{det} F - \overline{q}^{\tau 1} \right) p_w^* d\Gamma^{\tau 1} - W^{\tau 1} \tag{17}$$

where we assume that Q is position independent and that **det** F is the Jacobian determinant of $F_{ij} = \partial x_i^{\tau 2} / \partial x_j^{\tau 1}$, transporting scalars on large strains for mapping from $\Omega^{\tau 2}$ to $\Omega^{\tau 1}$.

[28] Let us define

$$du_j^{\tau 1} = x_j^{\tau 2} - x_j^{\tau 1} \tag{18}$$

$$dp_w^{\tau 1} = p_w^{\tau 2} - p_w^{\tau 1} \tag{19}$$

$$d\phi^{\tau 1} = \phi^{\tau 2} - \phi^{\tau 1} \tag{20}$$

$$d\rho_w^{\tau 1} = \rho_w^{\tau 2} - \rho_w^{\tau 1} \tag{21}$$

$$dS_{r,w}^{\tau 1} = S_{r,w}^{\tau 2} - S_{r,w}^{\tau 1} \tag{22}$$

$$dk_{r,w}^{\tau 1} = k_{r,w}^{\tau 2} - k_{r,w}^{\tau 1} \tag{23}$$

$$d\overline{q}^{\tau 1} = \overline{q}^{\tau 2} - \overline{q}^{\tau 1} \tag{24}$$

Using a Taylor expansion of equation (17) and discarding terms of degree greater than one yields after some algebra (for further details, see *Chambon et al.* [2001], *Chambon and Moullet* [2004], and *Collin et al.* [2006]) the following linearized equations:

This allows us to find the corrections of the displacement fields du_i and the corrections of the pore water pressure dp_w to be added to their respective current values to obtain an new current configuration and a new displacements and pore water pressures field closer to a well-balanced configuration.

[29] If we assume the following relationships coming from a linearization of equations (5) and (14), the preceding equation can be expressed as a function of the unknowns du_i and dp_w

$$d\rho_w^{\tau 1} = \frac{\rho_w^{\tau 1}}{\chi_w} dp_w^{\tau 1} \tag{26}$$

$$d\phi^{\tau 1} = \left(1 - \phi^{\tau 1} \right) \frac{d\Omega^{\tau 1}}{\Omega^{\tau 1}} = \left(1 - \phi^{\tau 1} \right) \frac{\partial du_m^{\tau 1}}{\partial x_m^{\tau 1}} \tag{27}$$

$$dS_{r,w}^{\tau 1} = \frac{\partial S_{r,w}^{\tau 1}}{\partial p_w^{\tau 1}} dp_w^{\tau 1} \tag{28}$$

$$dk_{r,w}^{\tau 1} = \frac{\partial k_{r,w}^{\tau 1}}{\partial S_{r,w}^{\tau 1}} \frac{\partial S_{r,w}^{\tau 1}}{\partial p_w^{\tau 1}} dp_w^{\tau 1} \tag{29}$$

$$\begin{aligned} d\overline{q}^{\tau 1} &= \alpha \left(d\rho_v^{f,\tau 1} - d\rho_v^{cav,\tau 1} \right) + 2\beta \left(p_w^{f,\tau 1} - p_w^{cav,\tau 1} \right) \\ &\quad \cdot \left(dp_w^{f,\tau 1} - dp_w^{cav,\tau 1} \right) \\ &= \left[\alpha \frac{\rho_{v,0} M_v}{RT \rho_w^{\tau 1}} \left(h^{f,\tau 1} - h^{cav,\tau 1} \right) + 2\beta \left(p_w^{f,\tau 1} - p_w^{cav,\tau 1} \right) \right] \\ &\quad \cdot \left(dp_w^{f,\tau 1} - dp_w^{cav,\tau 1} \right) \end{aligned} \tag{30}$$

$$\text{if} \quad p_w^f \geq p_w^{cav} \quad \textit{and} \quad p_w^f \geq p_{atm}$$

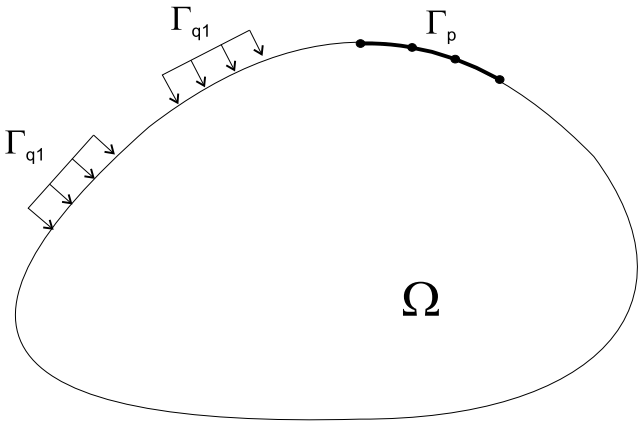

Figure 3. Flow boundary conditions.

[30] Linearization of the mechanical problem can be found in work by *Collin et al.* [2006] and gives

$$\int_{\Omega^{\tau 1}} \frac{\partial u_i^*}{\partial x_l^{\tau 1}} \left(d\sigma_{il}^{\tau 1} - \sigma_{ij}^{\tau 1} \frac{\partial du_l}{\partial x_j^{\tau 1}} + \sigma_{il}^{\tau 1} \frac{\partial du_m}{\partial x_m^{\tau 1}} \right) d\Omega^{\tau 1} - \int_{\Omega^{\tau 1}} u_i^* \left(\rho_{mix}^{\tau 1} \frac{\partial du_m}{\partial x_m^{\tau 1}} - \left(\rho_s^{\tau 1} - S_{r,w}^{\tau 1} \rho_w^{\tau 1} \right) d\phi^{\tau 1} + d\rho_w^{\tau 1} S_{r,w}^{\tau 1} \phi^{\tau 1} + dS_{r,w}^{\tau 1} \rho_w^{\tau 1} \phi^{\tau 1} \right) g_i d\Omega^{\tau 1} = -R^{\tau 1} \quad (31)$$

where $\rho_{mix}^{\tau 1}$ is the mass density of the mixture in configuration $\Omega^{\tau 1}$ ($\rho_{mix}^{\tau} = \rho_s^t(1-\phi^t) + S_{r,w}^t \rho_w^t \phi^t$), $R^{\tau 1}$ is the residual of the mechanical problem and $d\sigma_{il}^{\tau 1}$ can be linearized by

$$d\sigma_{il}^{\tau 1} = d\sigma_{il}'^{\tau 1} - S_{r,w}^{\tau 1} dp_w^{\tau 1} \delta_{il} - dS_{r,w}^{\tau 1} p_w^{\tau 1} \delta_{il} = C_{ilkj}^{\tau 1} \frac{\partial du_k^{\tau 1}}{\partial x_j^{\tau 1}} - S_{r,w}^{\tau 1} dp_w^{\tau 1} \delta_{il} - dS_{r,w}^{\tau 1} p_w^{\tau 1} \delta_{il} \quad (32)$$

where we assumed the Bishop's definition of effective stress tensor [*Nuth and Laloui*, 2008]. It should be pointed out that matrix $C_{iljk}^{\tau 1}$ is computed through a consistent linearization of the constitutive law integration algorithm [*Simo and Taylor*, 1985].

[31] Equations (25) and (31) have different contributions coming from geometrical nonlinear effects (since we distinguished $\Omega^{\tau 1}$ and $\Omega^{\tau 2}$ in the developments) and from the couplings between pore water pressure and the mechanical problem. These contributions will be highlighted in section 5, where the formulation of a coupled finite element and a boundary finite element are detailed.

5. Coupled 2-D Finite Element and Boundary Finite Element Formulations

[32] Classical boundary condition of flows problems are respectively the Dirichlet (imposed pressure) and the Neumann type (imposed flux). On the boundary of a body of volume Ω, we can impose the following classical boundary conditions (Figure 3): flux different from zero on the surface Γ_{q1}, pressure variations on the surface Γ_p, and impervious condition on $\Gamma_{q2} = \Gamma \backslash \{\Gamma_{q1} \cup \Gamma_p\}$.

[33] To reproduce the seepage and evaporation flows which occur near the tunnel surface, we need classical quadrilateral 2-D finite elements (to simulate the rock mass coupled behavior), associated with a new boundary finite element through which the hydraulic exchanges between cavity air and the formation take place. This boundary element is necessary because the seepage and evaporation flows correspond to nonclassical boundary condition. The special element has been developed in the finite element code Lagamine [*Collin*, 2003] and is defined by four nodes (Figure 4). The first three nodes are located on the boundary (N1, N2 and N3). They allow a spatial discretization of the pore water pressure distribution along the boundary. The

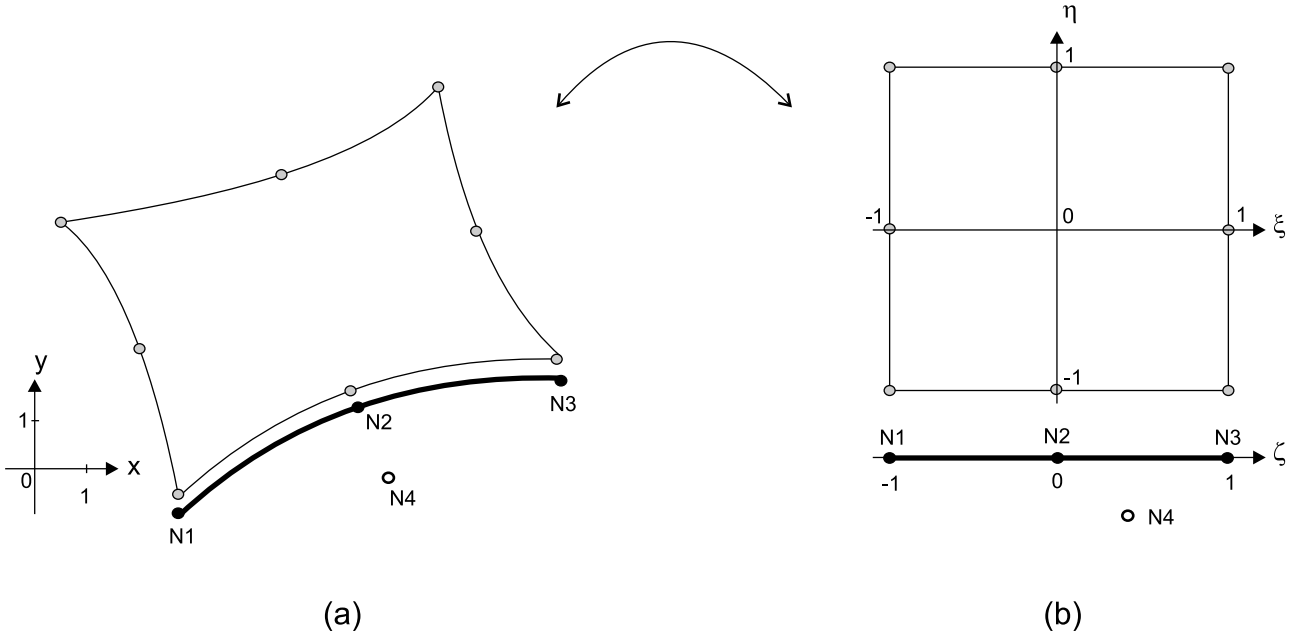

Figure 4. (a) Two-dimensional finite element and boundary element and (b) the corresponding parent elements.

fourth node is introduced to define the relative humidity in the cavity and its geometrical position does not influence the results (N4). The corresponding one-dimensional parent element is defined as a function of ζ ($-1 < \zeta < 1$). In the following, the finite element formulation of the problem is presented, with a special emphasize of the numerical description of the four-node boundary finite element.

[34] In order to define the local element stiffness matrix, equations (25) and (31) are rewritten in a matricial form:

$$\int_{\Omega^{\tau 1}} \left[U^{*,\tau 1}_{(x,y)}\right]^T \left[E^{\tau 1}\right] \left[dU^{\tau 1}_{(x,y)}\right] d\Omega^{\tau 1} = \int_{\Gamma^{\tau 1}_q} \left[U^{*,\tau 1}_{(x,y)}\right]^T \left[F^{\tau 1}\right] \left[dU^{\tau 1}_{(x,y)}\right] d\Gamma^{\tau 1}_q - R^{\tau 1} - W^{\tau 1} \tag{33}$$

where $[dU^{\tau 1}_{(x,y)}]$ is defined in equation (34) and $[U^{*,\tau 1}_{(x,y)}]$ has the same structure as the corresponding virtual quantities:

$$\left[dU^{\tau 1}_{(x,y)}\right]^T \equiv \left[\frac{\partial du^{\tau 1}_1}{\partial x^{\tau 1}_1} \frac{\partial du^{\tau 1}_1}{\partial x^{\tau 1}_2} \frac{\partial du^{\tau 1}_2}{\partial x^{\tau 1}_1} \frac{\partial du^{\tau 1}_2}{\partial x^{\tau 1}_2} du^{\tau 1}_1 du^{\tau 1}_2 \frac{\partial dp^{\tau 1}_w}{\partial x^{\tau 1}_1} \frac{\partial dp^{\tau 1}_w}{\partial x^{\tau 1}_2} dp^{\tau 1}_w\right] \tag{34}$$

[35] In equation (33), the left-hand term is computed by a 2-D coupled finite element and the first right-hand term is evaluated by the 1-D boundary finite element. The finite element spatial discretization is introduced in equation (33) using the transformation matrices $[T^{\tau 1}]$ and $[B]$ for the 2-D finite element (and respectively $[S^{\tau 1}]$ and $[C]$ for the boundary finite element), with connect $[dU^{\tau 1}_{(x,y)}]$ to the nodal variables $[dU^{\tau 1}_{Node}]$ (Figure 4):

$$\left[dU^{\tau 1}_{(x,y)}\right] = \left[T^{\tau 1}\right] \left[dU^{\tau 1}_{(\xi,\eta)}\right] \text{for the } 2-\text{D finite element} \tag{35}$$

$$\left[dU^{\tau 1}_{(x,y)}\right] = \left[S^{\tau 1}\right] \left[dU^{\tau 1}_{(\zeta)}\right] \text{ for the boundary finite element} \tag{36}$$

and

$$\left[dU^{\tau 1}_{(\xi,\eta)}\right] = [B] \left[dU^{2D,\tau 1}_{Node}\right] \text{ for the } 2-\text{D finite element} \tag{37}$$

$$\left[dU^{\tau 1}_{(\zeta)}\right] = [C] \left[dU^{BE,\tau 1}_{Node}\right] \text{ for the boundary finite element} \tag{38}$$

The usual one-dimensional quadratic Serendipity shape functions are used for the boundary finite element.

[36] Integration of equation (33) on finite element yields

$$\begin{aligned} &\left[U^{2D,*}_{node}\right]^T \int_{-1}^{1}\int_{-1}^{1} [B]^T \left[T^{\tau 1}\right]^T \left[E^{\tau 1}\right] \left[T^{\tau 1}\right] [B] \det J^{\tau 1} d\xi d\eta \left[dU^{2D,\tau 1}_{Node}\right] \\ &- \left[U^{BE,*}_{node}\right]^T \int_{-1}^{1} [C]^T \left[S^{\tau 1}\right]^T \left[F^{\tau 1}\right] \left[S^{\tau 1}\right] [C] \det L^{\tau 1} d\zeta \left[dU^{BE,\tau 1}_{Node}\right] \\ &\equiv \left[U^{2D,*}_{node}\right]^T \left[k^{2D,\tau 1}\right] \left[dU^{\tau 1}_{Node}\right] - \left[U^{BE,*}_{node}\right]^T \left[k^{BE,\tau 1}\right] \left[dU^{BE,\tau 1}_{Node}\right] \end{aligned} \tag{39}$$

where $[k^{2D,\tau 1}]$ and $[k^{BE,\tau 1}]$ are the local element stiffness matrices respectively of the 2-D finite element and of the boundary finite element, $J^{\tau 1}$ is the Jacobian matrix of the mapping from (ξ,η) to (x, y) for the 2-D finite element (and $L^{\tau 1}$ is the Jacobian matrix of the mapping from (ς) to (x, y) for the boundary finite element) and $[dU^{2D,\tau 1}_{Node}]$ and $[dU^{BE,\tau 1}_{Node}]$ have the following definition:

$$\left[dU^{2D,\tau 1}_{Node}\right]^T = \begin{bmatrix} du^{\tau 1}_{1(-1,-1)} du^{\tau 1}_{2(-1,-1)} dp^{\tau 1}_{w(-1,-1)} \times du^{\tau 1}_{1(-1,0)} du^{\tau 1}_{2(-1,0)} dp^{\tau 1}_{w(-1,0)} \times du^{\tau 1}_{1(-1,1)} du^{\tau 1}_{2(-1,1)} dp^{\tau 1}_{w(-1,1)} \\ \times du^{\tau 1}_{1(0,-1)} du^{\tau 1}_{2(0,-1)} dp^{\tau 1}_{w(0,-1)} \times du^{\tau 1}_{1(0,1)} du^{\tau 1}_{2(0,1)} dp^{\tau 1}_{w(0,1)} \times du^{\tau 1}_{1(1,-1)} du^{\tau 1}_{2(1,-1)} dp^{\tau 1}_{w(1,-1)} \\ \times du^{\tau 1}_{1(1,0)} du^{\tau 1}_{2(1,0)} dp^{\tau 1}_{w(1,0)} \times du^{\tau 1}_{1(1,1)} du^{\tau 1}_{2(1,1)} dp^{\tau 1}_{w(1,1)} \end{bmatrix} \tag{40}$$

$$\left[dU^{BE,\tau 1}_{Node}\right]^T = \left[du^{\tau 1}_{1(-1)} du^{\tau 1}_{2(-1)} dp^{\tau 1}_{w(-1)} \times du^{\tau 1}_{1(0)} du^{\tau 1}_{2(0)} dp^{\tau 1}_{w(0)} \times du^{\tau 1}_{1(1)} du^{\tau 1}_{2(1)} dp^{\tau 1}_{w(1)}\right] \tag{41}$$

[37] $[E^{\tau 1}]$ and $[F^{\tau 1}]$ are (9×9) matrixes that contain all the terms of equations (25) and (31), respectively for 2-D finite element (2D) and boundary finite element (BE):

$$\left[E^{\tau 1}\right] = \begin{bmatrix} K^{2D}_{MM^{\tau 1}_{(6\times 6)}} & K^{2D}_{WM^{\tau 1}_{(6\times 3)}} \\ K^{2D}_{MW^{\tau 1}_{(3\times 6)}} & K^{2D}_{WW^{\tau 1}_{(3\times 3)}} \end{bmatrix} \tag{42}$$

$$\left[F^{\tau 1}\right] = \begin{bmatrix} 0_{(6x6)} & 0_{(6x3)} \\ K^{BE}_{MW^{\tau 1}_{(3x6)}} & K^{BE}_{WW^{\tau 1}_{(3x3)}} \end{bmatrix} \tag{43}$$

Matrices K^{2D}_{WW} and K^{2D}_{MM} are the classical stiffness matrices for a flow and a mechanical problem with 2-D finite element. K^{2D}_{WM} and K^{2D}_{MW} contain all the couplings terms appearing between the mechanical problem and the flow one:

$$K^{2D}_{WW^{\tau 1}_{(3\times 3)}} = \begin{bmatrix} \rho^{\tau 1}_w \frac{\kappa k^{\tau 1}_{r,w}}{\mu_w} & 0 & C1 \\ 0 & \rho^{\tau 1}_w \frac{\kappa k^{\tau 1}_{r,w}}{\mu_w} & C2 \\ 0 & 0 & D \end{bmatrix} \tag{44}$$

$$K^{2D}_{MM^{\tau 1}_{(6\times 6)}} = \begin{bmatrix} C_{1111} & C_{1112}-\sigma^{\tau 1}_{12} & C_{1121} & C_{1122}+\sigma^{\tau 1}_{11} & 0 & 0 \\ C_{1211}+\sigma^{\tau 1}_{12} & C_{1212} & C_{1221}-\sigma^{\tau 1}_{11} & C_{2222} & 0 & 0 \\ C_{2111} & C_{2112}-\sigma^{\tau 1}_{22} & C_{2121} & C_{2122}+\sigma^{\tau 1}_{21} & 0 & 0 \\ C_{2211}+\sigma^{\tau 1}_{22} & C_{2212} & C_{2221}-\sigma^{\tau 1}_{21} & C_{2222} & 0 & 0 \\ G & 0 & 0 & G & 0 & 0 \\ G & 0 & 0 & G & 0 & 0 \end{bmatrix} \tag{45}$$

$$K^{2D}_{MW^{\tau 1}_{(3\times 6)}} = \begin{bmatrix} -\rho^{\tau 1}_w \frac{\kappa k^{\tau 1}_{r,w}}{\mu_w}\frac{\partial p^{\tau 1}_w}{\partial x^{\tau 1}_1} & m^{\tau 1}_2 & -\rho^{\tau 1}_w \frac{\kappa k^{\tau 1}_{r,w}}{\mu_w}\frac{\partial p^{\tau 1}_w}{\partial x^{\tau 1}_2} & -m^{\tau 1}_1 & 0 & 0 \\ -m^{\tau 1}_2 & -\rho^{\tau 1}_w \frac{\kappa k^{\tau 1}_{r,w}}{\mu_w}\frac{\partial p^{\tau 1}_w}{\partial x^{\tau 1}_1} & m^{\tau 1}_1 & -\rho^{\tau 1}_w \frac{\kappa k^{\tau 1}_{r,w}}{\mu_w}\frac{\partial p^{\tau 1}_w}{\partial x^{\tau 1}_2} & 0 & 0 \\ A+\dot{M}^{\tau 1} & 0 & 0 & A+\dot{M}^{\tau 1} & 0 & 0 \end{bmatrix} \tag{46}$$

$$K^{2D}_{WM^{\tau 1}_{(6\times 3)}} = \begin{bmatrix} 0 & 0 & -S^{\tau 1}_{r,w} - p^{\tau 1}_w \frac{\partial S^{\tau 1}_{r,w}}{\partial p^{\tau 1}_w} \\ 0 & 0 & 0 \\ 0 & 0 & 0 \\ 0 & 0 & -S^{\tau 1}_{r,w} - p^{\tau 1}_w \frac{\partial S^{\tau 1}_{r,w}}{\partial p^{\tau 1}_w} \\ 0 & 0 & -\left(\frac{\rho^{\tau 1}_w}{\chi_w} S^{\tau 1}_{r,w}\phi^{\tau 1} + \rho^{\tau 1}_w \frac{\partial S^{\tau 1}_{r,w}}{\partial p^{\tau 1}_w}\phi^{\tau 1}\right) g_1 \\ 0 & 0 & -\left(\frac{\rho^{\tau 1}_w}{\chi_w} S^{\tau 1}_{r,w}\phi^{\tau 1} + \rho^{\tau 1}_w \frac{\partial S^{\tau 1}_{r,w}}{\partial p^{\tau 1}_w}\phi^{\tau 1}\right) g_2 \end{bmatrix} \tag{47}$$

where

$$A = \rho^{\tau 1}_w \left(\left(1-\phi^{\tau 1}\right)\left(\frac{S^{\tau 1}_{r,w}}{\chi_w}\dot{p}^{\tau 1}_w + \dot{S}^{\tau 1}_{r,w}\right) + S^{\tau 1}_{r,w}\left(\frac{1}{\Delta t} - \frac{\dot{\Omega}^{\tau 1}}{\Omega^{\tau 1}}\right)\right) \tag{48}$$

$$C1 = \frac{\rho^{\tau 1}_w}{\chi_w}\frac{\kappa k^{\tau 1}_{r,w}}{\mu_w}\left(\frac{\partial p^{\tau 1}_w}{\partial x^{\tau 1}_1} + \rho^{\tau 1}_w g_1\right) + \rho^{\tau 1}_w \frac{\rho^{\tau 1}_w}{\chi_w}\frac{\kappa k^{\tau 1}_{r,w}}{\mu_w} g_1 + \rho^{\tau 1}_w \frac{\kappa}{\mu_w}\frac{\partial k^{\tau 1}_{r,w}}{\partial S^{\tau 1}_{r,w}} \cdot \frac{\partial S^{\tau 1}_{r,w}}{\partial p^{\tau 1}_w}\left(\frac{\partial p^{\tau 1}_w}{\partial x^{\tau 1}_1} + \rho^{\tau 1}_w g_1\right) \tag{49}$$

$$C2 = \frac{\rho^{\tau 1}_w}{\chi_w}\frac{\kappa}{\mu_w}\left(\frac{\partial p^{\tau 1}_w}{\partial x^{\tau 1}_2} + \rho^{\tau 1}_w g_2\right) + \rho^{\tau 1}_w \frac{\rho^{\tau 1}_w}{\chi_w}\frac{\kappa}{\mu_w} g_2 + \rho^{\tau 1}_w \frac{\kappa}{\mu_w}\frac{\partial k^{\tau 1}_{r,w}}{\partial S^{\tau 1}_{r,w}} \cdot \frac{\partial S^{\tau 1}_{r,w}}{\partial p^{\tau 1}_w}\left(\frac{\partial p^{\tau 1}_w}{\partial x^{\tau 1}_2} + \rho^{\tau 1}_w g_2\right) \tag{50}$$

$$D = \frac{\rho^{\tau 1}_w}{\chi_w}\frac{\phi^{\tau 1}}{\chi_w} S^{\tau 1}_{r,w}\dot{p}^{\tau 1}_w + \rho^{\tau 1}_w \frac{\phi^{\tau 1}}{\chi_w}\frac{S^{\tau 1}_{r,w}}{\Delta t} + \rho^{\tau 1}_w \frac{\phi^{\tau 1}}{\chi_w}\frac{\partial S^{\tau 1}_{r,w}}{\partial p^{\tau 1}}\dot{p}^{\tau 1}_w + \frac{\rho^{\tau 1}_w}{\chi_w}\phi^{\tau 1}\dot{S}^{\tau 1}_{r,w} + \rho^{\tau 1}_w \frac{\phi^{\tau 1}}{\Delta t}\frac{\partial S^{\tau 1}_{r,w}}{\partial p^{\tau 1}_w} + \frac{\rho^{\tau 1}_w}{\chi_w} S^{\tau 1}_{r,w}\frac{\dot{\Omega}^{\tau 1}}{\Omega^{\tau 1}} + \rho^{\tau 1}_w \frac{\partial S^{\tau 1}_{r,w}}{\partial p^{\tau 1}_w}\frac{\dot{\Omega}^{\tau 1}}{\Omega^{\tau 1}} \tag{51}$$

$$G = -\rho^{\tau 1}_{mix} + \left(\rho_s - S^{\tau 1}_{r,w}\rho^{\tau 1}_w\right)\left(1-\phi^{\tau 1}\right) \tag{52}$$

Matrices K^{BE}_{WW} and K^{BE}_{MW} contain all the terms appearing because of the dependence of the total boundary flow $\overline{q}^t$ with displacement and hydraulic field. These stiffness matrices of the boundary element are detailed hereafter.

$$K^{BE}_{WW^{\tau 1}_{(3\times 3)}} = \begin{bmatrix} 0 & 0 & 0 \\ 0 & 0 & 0 \\ 0 & 0 & Z \end{bmatrix} \tag{53}$$

$$K^{BE}_{MW^{\tau 1}_{(3\times 6)}} = \begin{bmatrix} 0 & 0 & 0 & 0 & 0 & 0 \\ 0 & 0 & 0 & 0 & 0 & 0 \\ \overline{q}^{\tau 1} & 0 & 0 & \overline{q}^{\tau 1} & 0 & 0 \end{bmatrix} \tag{54}$$

with

$$Z = \begin{cases} \left[\alpha\frac{\rho_{v,0}M_v}{RT\rho^{\tau 1}_w}\left(h^{f,\tau 1} - h^{cav,\tau 1}\right) + 2\beta\left(p^{f,\tau 1}_w - p^{cav,\tau 1}_w\right)\right] \\ \quad if\ p^f_w \geq p^{cav}_w\ and\ p^f_w \geq p_{atm} \\ \left[\alpha\frac{\rho_{v,0}M_v}{RT\rho^{\tau 1}_w}\left(h^{f,\tau 1} - h^{cav,\tau 1}\right)\right] \\ \quad if\ p^f_w < p^{cav}_w\ or\ p^f_w < p_{atm} \end{cases} \tag{55}$$

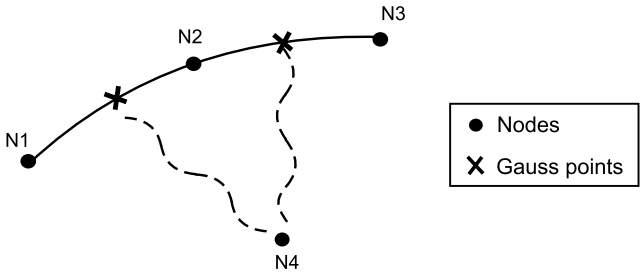

Figure 5. Boundary finite element description.

In equation (33), the residual terms $R^{\tau 1}$ and $W^{\tau 1}$ are computed for each element thanks to the following relationship:

$$-R^{\tau 1} - W^{\tau 1} = P_e^{t*} - \left[U_{node}^{2D,*}\right]^T \int_{-1}^{1}\int_{-1}^{1} [B]^T [T^t]^T \left[\sigma^{2D,t}\right] \det J^t d\xi d\eta + \left[U_{node}^{BE,*}\right]^T \int_{-1}^{1} [C]^T [S^t]^T \left[\sigma^{BE,t}\right] \det L^t d\zeta \equiv \left[U_{node}^{2D,*}\right]\left[f_{HE}^{2D,t}\right] + \left[U_{node}^{BE,*}\right]\left[f_{HE}^{BE,t}\right] \quad (56)$$

$$\left[\sigma^{2D,\tau 1}\right]^T = \left[\sigma_{11}^{\tau 1} \quad \ldots \quad \sigma_{22}^{\tau 1} \quad -m_1^{\tau 1} \quad -m_2^{\tau 1} \quad \dot{M}^{\tau 1}\right] \quad (57)$$

$$\left[\sigma^{BE,\tau 1}\right] = \left[\overline{q}^{\tau 1}\right] \quad (58)$$

where $[f_{HE}^{2D,t}]$ and $[f_{HE}^{BE,t}]$ are the elementary out of balance forces respectively for the 2-D finite element and for the boundary finite element. The external virtual power P_e^{t*} contains the contributions of the body forces (for the mechanical and the flow problems), except the term related to gravity volume force, which is introduced in the $[\sigma^{2D,\tau 1}]$ vector.

[38] It is worth mentioning that the integration procedure of equations (39) and (56) uses Gauss method. In order to avoid possible locking in the plastic range, the 2-D elements are underintegrated, which means here that only four Gauss points are used. Concerning the boundary finite element, two Gauss points are considered (Figure 5). The exchange flow $\overline{q}^t$ is computed thank to equation (14), where the cavity relative humidity is computed with the pressure of the fourth node (N4) and the rock mass relative humidity is evaluated at the Gauss points.

[39] The global stiffness matrix and out of balance force can be obtained by assembling the elementary matrices given by equations (39) and (56). After solving the resulting auxiliary linear system, a new configuration is found and the equilibrium is checked. A monolithic procedure is chosen where the full stiffness matrix is computed at each iteration of the Newton-Raphson procedure.

6. Numerical Modeling of an Excavation

[40] For the design of nuclear waste disposals in deep geological layer, a correct numerical modeling of the coupled processes occurring during cavities excavations is needed. In order to evidence the influence of the hydraulic boundary condition, the excavation of a cylindrical cavity located in a homogeneous low-permeability formation is modeled. The geometry and the mechanical law used in the following are those proposed in the GdR-MoMaS benchmark exercise [*Chavant and Fernandez*, 2005]. The mechanical constitutive model corresponds to a highly dilatant material. In such conditions, the coupling effects between the mechanical law and the flow problem are enhanced.

[41] A 3 m diameter cylindrical unsupported cavity is located in a homogeneous low- permeability formation. The excavation process lasts for 1.5×10^6 s (around 17 days) and is modeled by a progressive decrease of the initial total stress and pore water pressure down to the atmospheric pressure. An initial isotropic stress state allows one dimensional axisymmetrical modeling: $\sigma_r' = 7$ MPa and $p_w = 5$ MPa. Two steps are considered in the modeling: first the excavation process (duration $T_c = 1.5 \times 10^6$ s) and a second phase during which the radial convergence of the cavity evolves because of the water diffusion process. The final modeling time is 300×10^6 s (about 9.5 years). At the external boundaries of our model, the initial conditions are assumed to be preserved in terms of total stress and pore water pressure. The external radius is seven times the internal one. At this distance, the external boundary conditions have a small influence on the cavity convergence. At the inner wall, the boundary conditions are the following:

$$\begin{cases} for\ 0 \le t \le T_c : \sigma_r = \sigma_r' - S_{r,w} p_w = \sigma^0 \left(1 - \dfrac{t}{T_c}\right) \\ \quad + 0.1\,MPa\ and\ p_w = 5\left(1 - \dfrac{t}{T_c}\right) + 0.1\,MPa \\ for\ t > T_c : \sigma_r = p_w = 0.1\,MPa \end{cases} \quad (59)$$

The conditions are isothermal ($T = 293$°K) and gas pressure is assumed constant (equal to the atmospheric pressure).

6.1. Mechanical Constitutive Model

[42] In order to reproduce the progressive decrease of the material strength, the mechanical constitutive law previously proposed for GdR-Momas benchmark exercises [*Chavant and Fernandez*, 2005] is used. This constitutive law is an elastoplastic strain-softening model using the associated Drucker-Prager yield criterion given by the following equation:

$$F \equiv \sqrt{\frac{3}{2}} II_{\hat{\sigma}} + m\left(I_\sigma - \frac{3c}{\tan\varphi}\right) = 0 \quad (60)$$

where $II_{\hat{\sigma}}$ is the second deviatoric stress invariant, I_σ is the first stress invariant, ϕ is the friction angle, parameter m is a function of ϕ: $m = \frac{2\sin(\varphi)}{2-\sin(\varphi)}$, the cohesion $c = c_0 f(\gamma^p)$ is the softening variable, c_0 is the initial cohesion and γ^p is the equivalent deviatoric plastic deformation.

Table 1. Parameters of the Mechanical Model

	Description	Value	Units
E_0	Young modulus	5800	MPa
υ_0	Poisson ratio	0.3	-
c_0	initial cohesion	1	MPa
ϕ	friction angle	25	deg
θ	residual cohesion	0.01	-
γ_R^p	deviatoric strain threshold	0.015	-

Table 2. Parameters of the Flow Model

	Description	Value	Units
κ	intrinsic permeability	10^{-19}	m^2
$\rho_{w,0}$	water density	1000	kg/m^3
ϕ_0	initial porosity	0.15	-
χ_w	water bulk modulus	2000	MPa
μ_w	water dynamic viscosity	0.001	Pa s

[43] Because of the associated plastic law, the behavior of the material is highly dilatant, which increases the coupling effects between the mechanical and the flow problem. The evolution of the cohesion is related to the equivalent plastic deformation through the following relationship:

$$\begin{aligned} f(\gamma^p) &= \left(1-(1-\theta)\frac{\gamma^p}{\gamma_R^p}\right)^2 \quad \text{if } 0<\gamma^p<\gamma_R^p \\ f(\gamma^p) &= \theta^2 \qquad\qquad\qquad\quad \text{if } \gamma^p \geq \gamma_R^p \end{aligned} \tag{61}$$

where θ is a parameter controlling the residual value of cohesion and γ_R^p is the equivalent deviatoric plastic deformation, for which the residual value of cohesion is reached. The following modeling has been performed with the parameters values defined in Table 1.

6.2. Hydraulic Properties

[44] The relationships describing the hydraulic behavior have been developed in section 2.2. The following parameters have been used in the modeling of the cavity excavation (Table 2).

[45] The retention curve of the medium [*van Genuchten*, 1984] and the water relative permeability function [*Chavant and Fernandez*, 2005] are given by the following relationships (Figure 6):

$$S_{r,w} = \left[1+(\alpha p_c)^{\frac{1}{1-m}}\right]^{-m} \text{ and } S_{r,w}=1 \text{ if } p_c<0 \tag{62}$$

$$k_{r,w} = \left[1+\left(S_{r,w}^{-d}-1\right)^r\right]^{-1} \tag{63}$$

with $S_{r,w}$ the water relative saturation, $k_{r,w}$ the water relative permeability, p_c the capillary pressure, $\alpha = 10^{-7}$ Pa^{-1}, $m = 0.412$, $d = 2.429$ and $r = 1.176$.

6.3. Reference Case

[46] In this axisymmetrical modeling, we present respectively the pore water pressure distribution at four different time steps and the water outflow in the cavity (negative values mean an injection of water in the medium). In Figure 7a, we see that the pore water pressure remains (at the cavity wall) at the atmospheric pressure after the excavation phase. Because of the hydromechanical coupling (dilatancy effect), a negative pore water pressure is observed in the damaged zone, which implies an unphysical 'numerical' injection of water into the formation (Figure 7b).

[47] Figures (7c–7d) show the radial displacement distribution at four different time steps and the stress path followed in the first finite element at the wall. We see (Figure 7d) that the behavior is first elastic before the stress state reaches the initial yield surface. Because of the strain-softening, the cohesion decreases with a plastic dilatancy. At the end of the modeling, the stress state tends to zero as no more deviatoric stresses are allowed. The radial displacement (Figure 7c) is equal to 1.75 cm at the end of the excavation and reaches 21.2 cm after 300×10^6 s. The coupling effects between the water diffusion and the mechanical process are thus important.

6.4. Influence of the Hydraulic Boundary Condition

[48] If we consider that air ventilation in the cavity is sufficiently active to maintain constant the air relative humidity, we can imagine that after excavation, for long-term predictions, a thermodynamical equilibrium might be reached between the cavity air and the geological formation. One can assume equilibrium between the pore water pressure at the tunnel and the relative humidity of the cavity atmosphere. A second case (case 2) is then considered, where a relative humidity of 0.96 (corresponding to a negative pore water pressure of -5 MPa) is imposed at the cavity wall as a hydraulic boundary condition. Figure 8a shows the resulting pore water pressure which becomes negative at the cavity wall at the end of the excavation. After this first phase, the pore water pressure at the cavity wall remains negative as it is imposed by the boundary condition and the suction diffuses into the formation. In this case, we assist to a water outflow from the rock mass to the cavity to reach the imposed relative humidity at the wall. However, with other constitutive parameters, which should

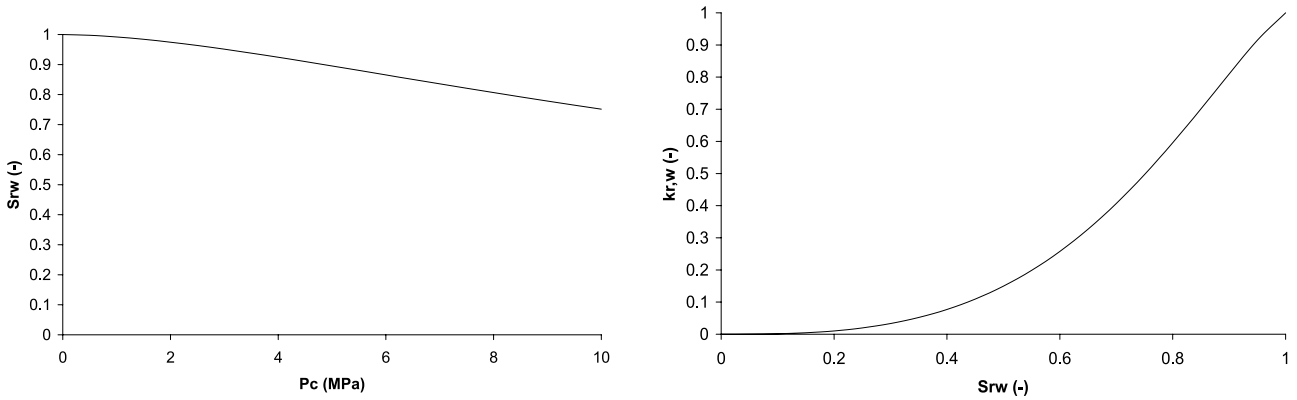

Figure 6. Retention and water relative permeability curves.

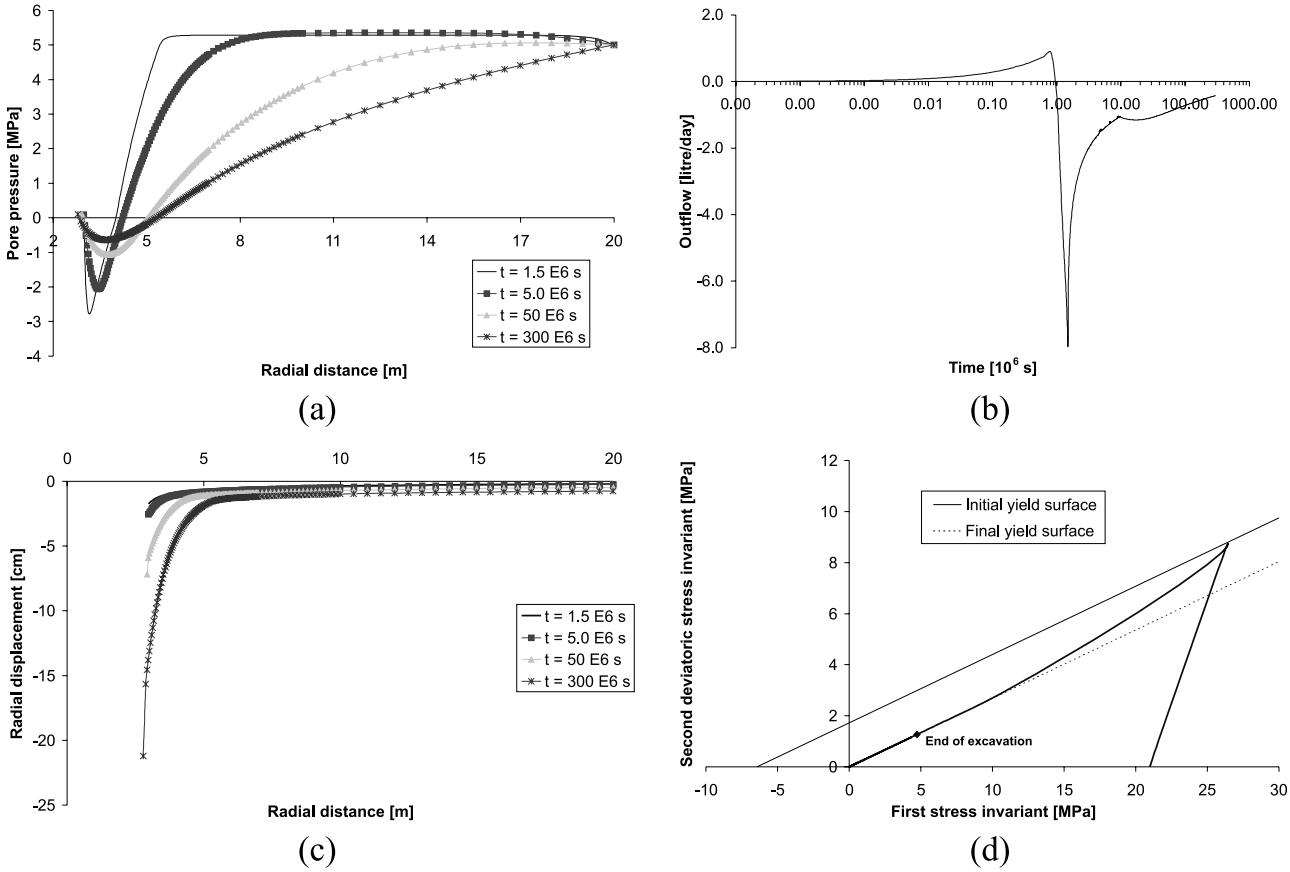

Figure 7. Case 1 (reference case) (a) pore water pressure distribution, (b) outflow evolution, (c) displacement evolution, and (d) stress path curve.

be more and more dilatant, water injection could neither be avoided.

[49] A third case (case 3) is then considered, using a seepage boundary condition: a liquid water outflow can be created only if the pore water pressure in the formation is higher than the atmospheric pressure and than the water pressure in the cavity (unilateral flow condition), as defined by equation (7). The relative humidity of the cavity air is decreased to 96 % during excavation and then remains constant to reproduce HR conditions of the tunnel. The seepage transfer coefficient β of equation (7) is assumed equal to 10^{-7} s^3 kg^{-1}. In term of pore water pressure profiles (Figure 9a), the results are similar at the end of the excavation to those in case 2. For long-term predictions, pore water pressure progressively increases at the wall to reach the atmospheric pressure. Water outflows between geological formation and the cavity are now realistic, because only outflows are possible. But the equilibrium between the pore water pressure at the wall and the relative humidity in the cavity atmosphere is not reached in this case. Indeed, Figure 9b presents the temporal evolution of rock mass and cavity relative humidities. During excavation, the cavity air relative humidity decreases and then remains constant till the end of the modeling, considering the sufficiently active air ventilation. In the rock mass, the relative humidity decreases during the excavation because of dilatancy effects. As far as the relative humidity is lower than one, no liquid outflow occurs. Thus, for long time predictions, the water pressure progressively increases because of the water flows coming from the formation.

[50] These two cases highlight the need of a more detailed expression of the water exchanges between the cavity atmosphere and the tunnel wall. In the fourth modeling (case 4), a mixed boundary condition with seepage and evaporation flows is thus used, as defined in equation (14). The results depend on the vapor mass transfer coefficient, defined in equation (8). *Ghezzehei et al.* [2004] have estimated the boundary layer thickness for different conditions (closed cavity, active or nonactive ventilation). The corresponding mass transfer coefficient varies between 10^{-3} m s^{-1} for closed tunnel to 4×10^{-3} m s^{-1} for active ventilation. We propose here to consider three values of mass transfer coefficient.

[51] With a small vapor transfer coefficient (case 4-1, $\alpha = 10^{-4}$ m s^{-1}), only seepage flows have influence on the flow boundary condition. The pore water pressure values (Figure 10a) tend to the atmospheric pressure at the wall. The profiles are thus similar to those using only seepage boundary condition (case 3, Figure 9a). Figure 10b shows that the equilibrium between the cavity atmosphere and the cavity wall in term of relative humidity is not reached at the end of the modeling.

[52] Using 100 times larger mass transfer coefficient (case 4-2, $\alpha = 10^{-2}$ m s^{-1}), the evaporation flow becomes preponderant on the seepage flow. Pore water pressure remains negative and close to the imposed water pressure

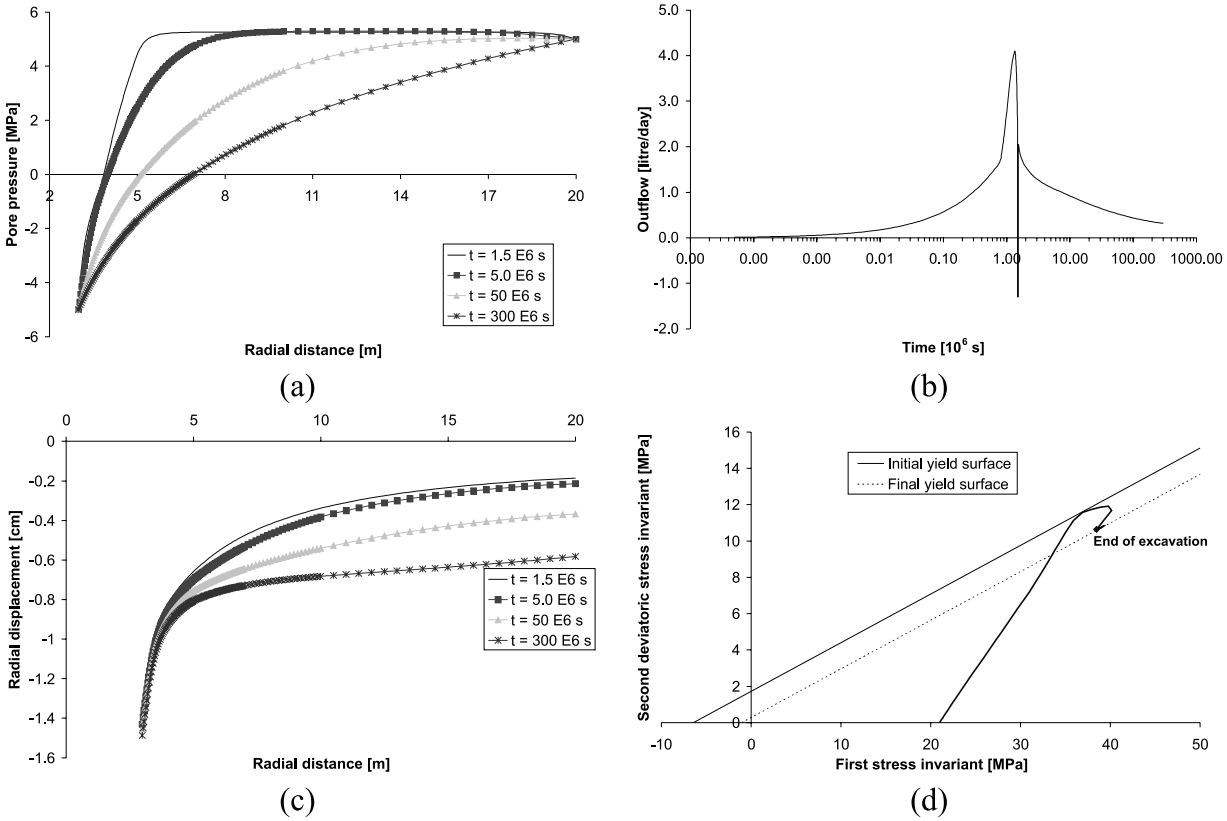

Figure 8. Case 2 (a) pore water pressure distribution, (b) outflow evolution, (c) displacement evolution, and (d) stress path curve.

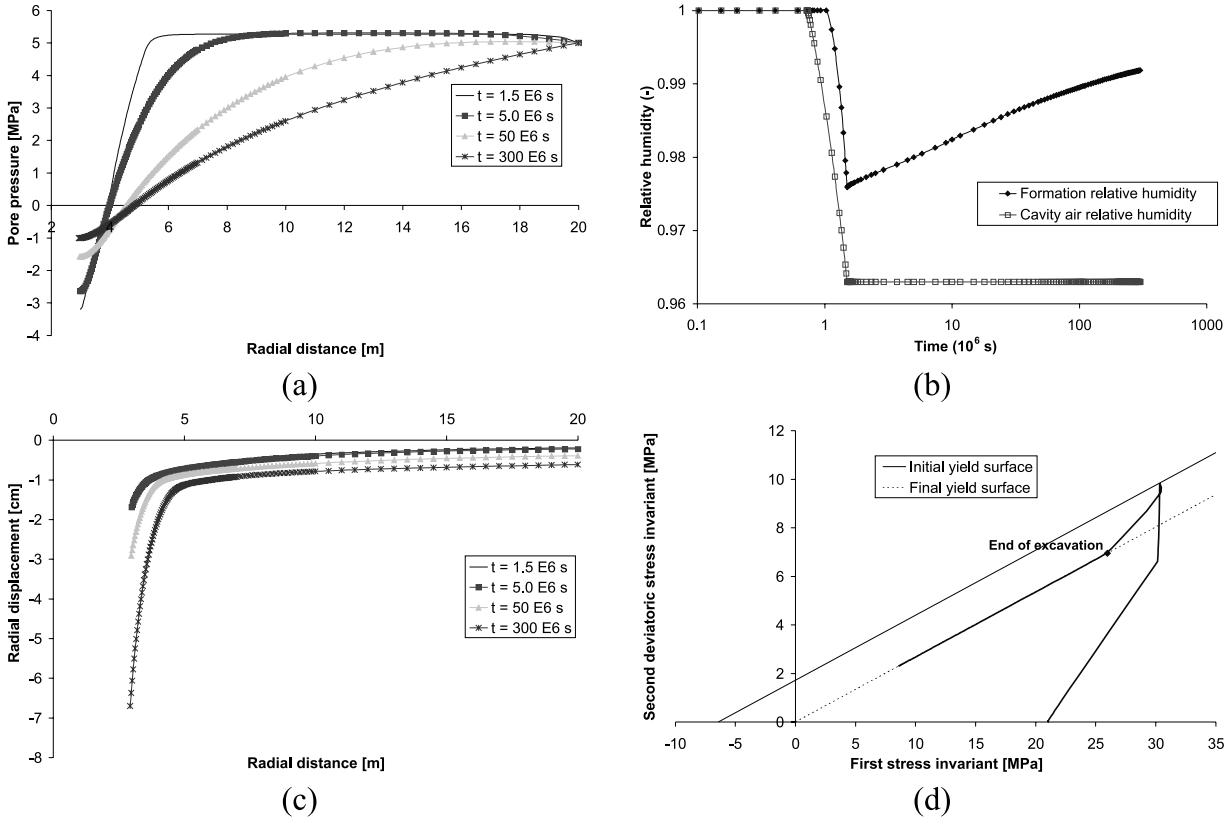

Figure 9. Case 3 (a) pore water pressure distribution, (b) relative humidity evolution, (c) displacement evolution, and (d) stress path curve.

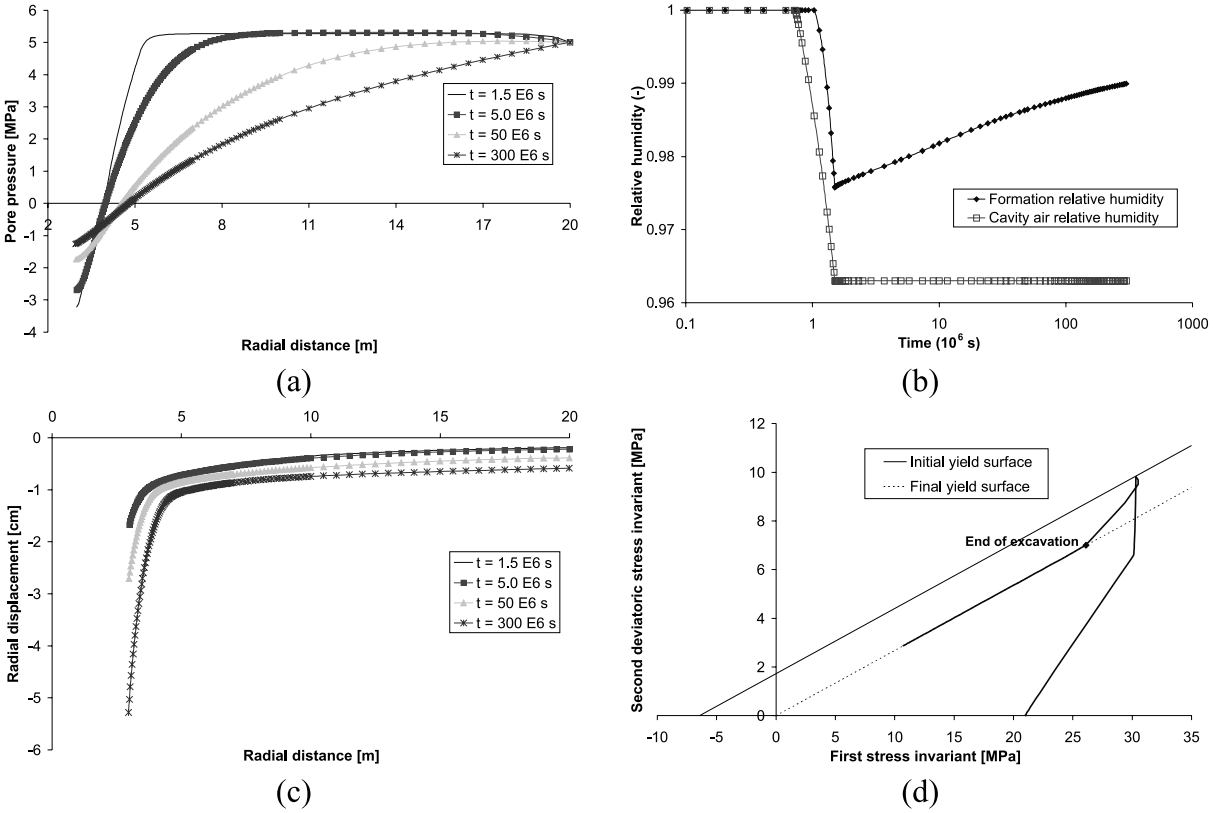

Figure 10. Case 4-1 (a) pore water pressure distribution, (b) relative humidity evolution, (c) displacement evolution, and (d) stress path curve.

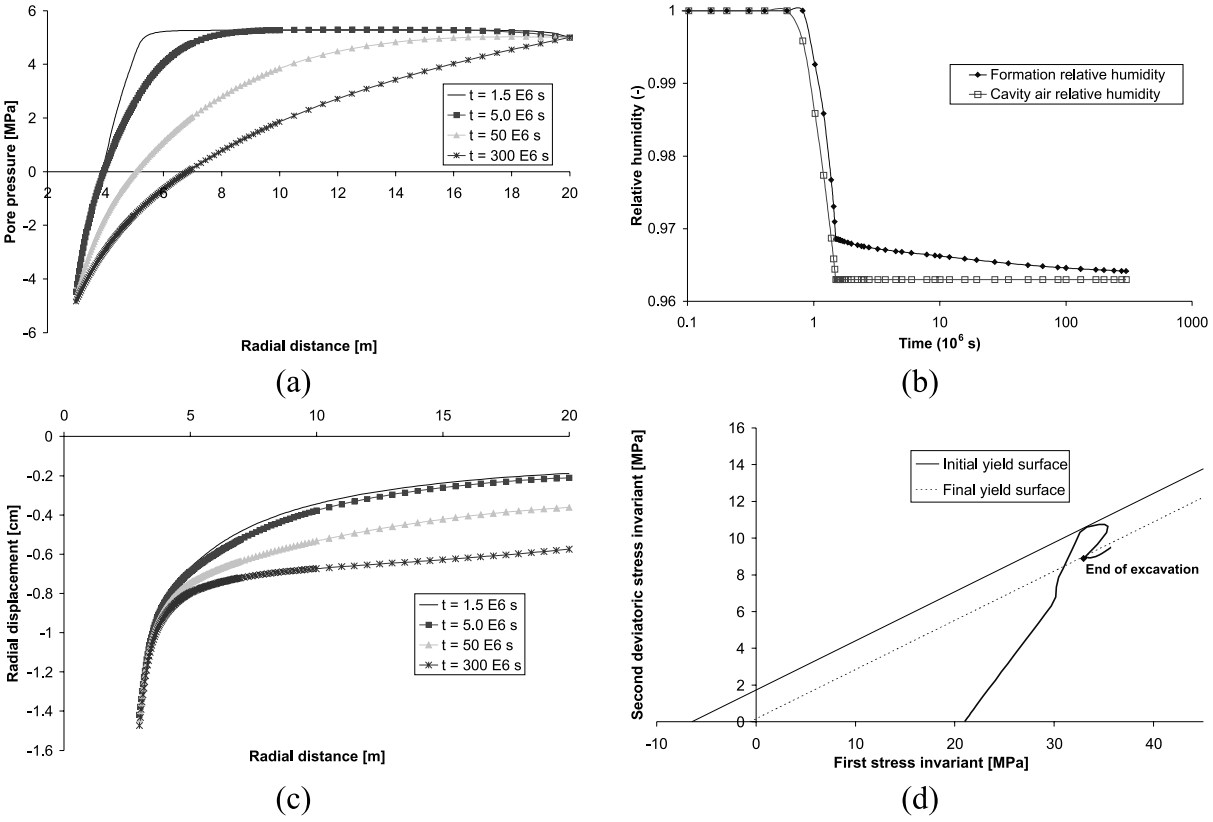

Figure 11. Case 4-2 (a) pore water pressure distribution, (b) relative humidity evolution, (c) displacement evolution, and (d) stress path curve.

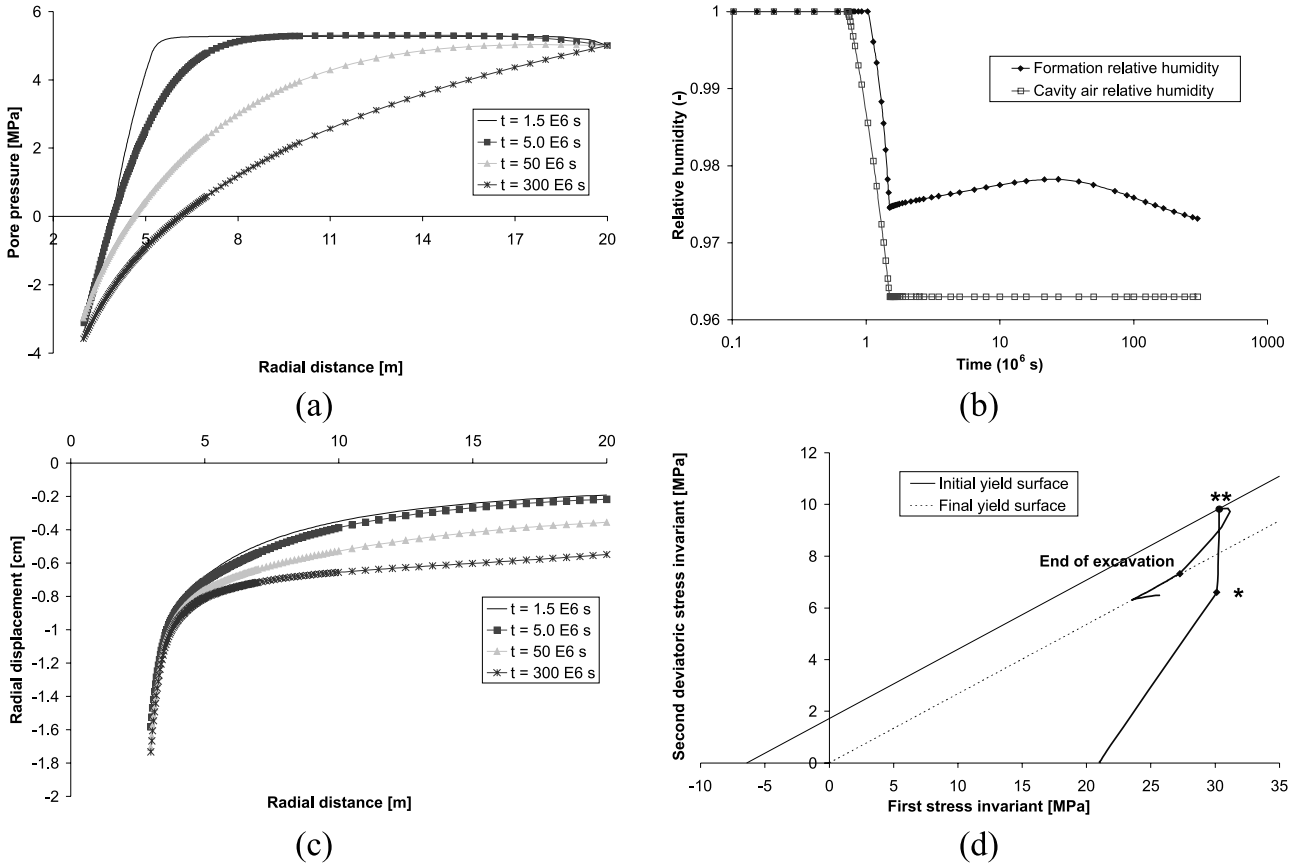

Figure 12. Case 4-3 (a) pore water pressure distribution, (b) relative humidity evolution, (c) displacement evolution, and (d) stress path curve.

in the cavity atmosphere (Figure 11a). The equilibrium between the relative humidity at the tunnel wall and in the cavity atmosphere is then quickly reached, as shown In Figure 11b. The pore water pressure profiles in the formation are quite similar to those obtained when a relative humidity (corresponding to a negative pore water pressure of -5 MPa) is imposed at the cavity wall as a boundary condition (case 2, Figure 8a).

[53] With an intermediate value of vapor mass transfer coefficient α equal to 10^{-3} m s^{-1} (case 4-3), seepage and evaporation flows are both influent. Pore water pressures at the wall (Figure 12d) are stabilized around -3 MPa. This pressure is an intermediate value between those obtained in case 4-1 and case 4-2.

[54] These different pore water pressure distributions have a direct influence on the predicted convergence. Table 3 presents the cavity convergence in the four cases. At the end of the excavation, the convergences are more or less the same. But as far as the long-term response is concerned, the predicted displacements are rather different. Indeed in case 2 (imposed humidity at the wall), the remaining suction near the tunnel ensures an additional strength and limits the material deformations. The case 4-2 (mixed flow condition with high vapor transfer coefficient) is quite similar to case 2. The stress paths followed in the first finite element near the wall confirm these results. Indeed, Figures 8d and 11d present more or less the same stress states at the end of the excavation and after 300×10^6 s. The geological formation recovers an elastic behavior at the end of the modeling and the high final value of the deviatoric stress is an indicator of the low plastic deformations. It is also interesting to note that the stress state does not evolve after the excavation when suction is imposed at the wall.

[55] With the seepage flow condition (case 3) or mixed flow condition with small vapor transfer coefficient (case 4-1), the stress paths are similar and the convergences obtained too. Figures 9d and 10d show that the residual value of cohesion is reached and the behavior is still plastic at the end of the modeling. The final value of the deviatoric stress is slightly higher than in case 1, so that the convergence is higher. It is also interesting to note that the stress paths become purely deviatoric (constant mean stress) during excavation when atmosphere in the tunnel begins to be unsaturated. Indeed, in this case, the seepage flows vanish and the flow boundary condition becomes undrained.

[56] In the case 4-3 (mixed flow condition with an intermediate mass transfer coefficient), the deviatoric stress decreases after the end of the excavation and the final stress state is located in the elastic domain (Figure 12d). Figure 13 presents the temporal evolution of the total, seepage and

Table 3. Cavity Convergence for Different Cases

	Case 1, cm	Case 2, cm	Case 3, cm	Case 4-1, cm	Case 4-2, cm	Case 4-3, cm
1.5×10^6 s	1.75	1.34	1.50	1.50	1.41	1.48
300×10^6 s	21.2	1.49	6.69	5.28	1.47	1.73

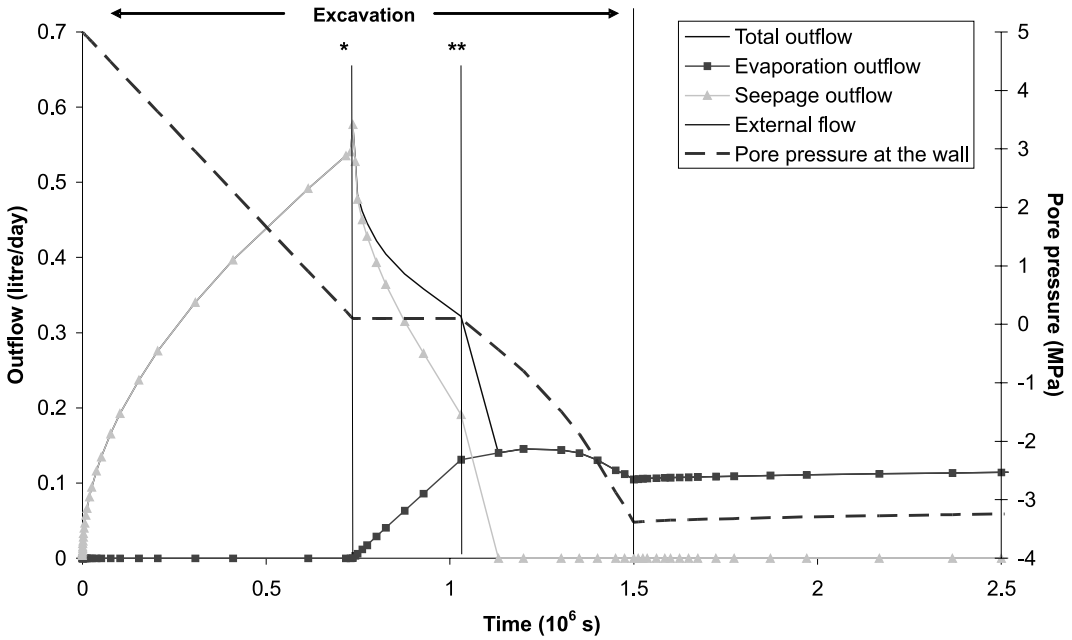

Figure 13. Case 4-3 temporal evolution of outflows and pore water pressure at the wall evolution (line with one asterisk, rock mass desaturation; line with two asterisks, entry in plasticity).

evaporation outflows, and the pore water pressure evolution at the wall of the tunnel as well. During the first part of the excavation, only seepage flow is active. When the atmosphere in the tunnel begins to be desaturated, the stress path evolves with constant mean stress, as shown previously in case 4-1. As a consequence, pore water pressure near the tunnel stabilizes. When the initial yield surface is reached, the pore water pressures decrease because of the highly dilatant behavior of the material. Seepage flow vanishes and evaporation flow becomes thus predominant.

[57] In the reference case (case 1), the excavated damage zone (EDZ) extends on 2.1 times the internal radius. With the mixed flow condition (case 4-1/3), the modeling predicts a rather narrow EDZ in comparison with case 1. However, the EDZ in cases 4-1, 4-2 and 4-3 are quite similar (between 1.71 and 1.74 times the internal radius), which means that the mass transfer coefficient has a small influence on the extent of the EDZ. The intensity of the plastic deformations within the EDZ is not the same for the three cases; the corresponding cavity convergences are thus different.

7. Discussions and Conclusions

[58] For the design of nuclear waste disposals in deep geological layer, a correct numerical prediction of the coupled processes occurring during theses excavations is needed. With the strain-softening constitutive model used, the coupling effects between water diffusion and the mechanical aspects are enhanced. After the description of the equations used in the finite element code, the modeling has shown that the flow boundary condition at the cavity wall deeply influences the cavity convergence.

[59] Four different kinds of boundary conditions are considered: wall pressure decreased down to the atmospheric pressure, suction imposed at the wall of the tunnel, seepage condition and a new boundary condition mixing seepage and evaporation flows. In low-permeability and highly dilatant medium, the case 1 leads to unphysical phenomenon, as the model predicts a massive injection of water into the formation. The case 2 predicts a small radial displacement as the suction is imposed as soon as the excavation is achieved. This hypothesis is very optimistic. With the seepage condition (case 3), the water may only flow into the cavity when pore water pressure is larger than the atmospheric pressure. This means that the equilibrium is never reached between the air humidity and the pore water pressure at the cavity wall. The conclusions for these three kinds of boundary conditions highlight the need of this fourth boundary condition, mixing two modes of exchange: seepage flow and vapor flow. Depending on the vapor transfer coefficient, the modeling predicts cavity convergences, from a small value (for high mass transfer coefficient) to large one (for small mass transfer coefficient). The modeling has shown that the proposed non classical boundary condition is able to predict the water exchanges occurring at the cavity wall under air ventilation. The coupled hydromechanical computations have also evidenced the influence of this flow boundary condition on the damage around the cavity.

Notation

c	cohesion (Pa).
$\overline{E}$	vapor exchange flow (kg m^{-2} s^{-1}).
E_0	Young modulus (Pa).
g	gravity acceleration (m s^2).
h	relative humidity (-).
I_σ	first stress invariant (Pa).
$II_{\hat{\sigma}}$	second deviatoric stress invariant (Pa).
$k_{r,w}$	water relative permeability (-).
m	mass flow (kg m^{-2} s^{-1}).
M	mass of the liquid water phase (kg m^{-3}).
M_v	vapor molar mass (kg mol^{-1}).
p_{atm}	atmospheric pressure (Pa).

p_c capillary pressure (Pa).
$p_{v,0}$ saturated vapor pressure (Pa).
p_w pore water pressure (Pa).
$\overline{q}$ water mass flow imposed on a boundary surface (kg m^{-2} s^{-1}).
Q sink term (kg s^{-1} m^{-3}).
R molar gas constant (J mol^{-1} kg^{-1}).
$\overline{S}$ seepage flow (kg m^{-2} s^{-1}).
$S_{r,w}$ water relative saturation (-).
t time (s).
$\overline{t}$ stress imposed on a boundary surface (Pa).
T_c drilling time (s).
T absolute temperature (°K).
u_i kinematically admissible virtual displacement (m).
α vapor mass transfer coefficient (m s^{-1}).
β seepage transfer coefficient (s^3 kg^{-1}).
γ^p equivalent deviatoric plastic deformation (-).
γ^p_R equivalent deviatoric plastic deformation threshold (-).
ε_{ij} strain tensor (-).
θ parameter controlling the residual value of cohesion (-).
κ intrinsic permeability (m^2).
μ_w water dynamic viscosity (Pa s).
ν_0 Poisson ratio (-)
ρ_s solid grain density (kg m^{-3}).
ρ_v vapor density (kg m^{-3}).
$\rho_{v,0}$ saturated vapor density (kg m^{-3}).
ρ_w water density (kg m^{-3}).
σ_{ij} stress tensor (Pa).
σ'_{ij} effective stress tensor (Pa).
Γ boundary of a volume (m).
φ friction angle (°).
ϕ porosity (-).
χ_w water bulk modulus (Pa).
Ω total volume (m^3).
Ω^v porous volume (m^3).

[60] **Acknowledgments.** The authors would like to thank the FRS-FNRS and the European project TIMODAZ for their financial support. TIMODAZ is cofunded by the European Commission (EC) as part of the sixth Euratom research and training Framework Programme (FP6) on nuclear energy (2002–2006). F.C. is a research associate at FNRS.

References

Anagnostou, G. (1995), Seepage flow around tunnels in swelling rock, *Int. J. Numer. Anal. Methods Geomech.*, *19*, 705–724, doi:10.1002/nag.1610191004.

Bardet, J. P., and T. Tobita (2002), A practical method for solving free-surface seepage problems, *Comput. Geotech.*, *29*, 451–475, doi:10.1016/S0266-352X(02)00003-4.

Ben Nasrallah, S., and P. Pere (1988), Detailed study of a model of heat and mass transfer during convective drying of porous media, *Int. J. Heat Mass Transfer*, *31*(5), 957–967, doi:10.1016/0017-9310(88)90084-1.

Borja, R., and E. Alarcon (1995), A mathematical framework for finite strain elastoplastic consolidation part 1: Balance law, variational formulation and linearization, *Comput. Methods Appl. Mech. Eng.*, *122*, 145–171, doi:10.1016/0045-7825(94)00720-8.

Brezis, H., D. Kinderlehrer, and G. Stampacchia (1978), Sur une nouvelle formulation du probleme de l'ecoulement a travers une digue, *C.R. Acad. Sci. Ser. A*, *287*, 711–714.

Chambon, R., and J. C. Moullet (2004), Uniqueness studies in boundary value problems involving some second gradient models, *Comput. Methods Appl. Mech. Eng.*, *193*, 2771–2796, doi:10.1016/j.cma.2003.10.017.

Chambon, R., S. Crochepeyre, and R. Charlier (2001), An algorithm and a method to search bifurcation points in non-linear problems, *Int. J. Numer. Methods Eng.*, *51*, 315–332, doi:10.1002/nme.199.

Chavant, C., and R. Fernandez (2005), Evaluating the reliability of hydro-mechanical simulation: A benchmark of numerical techniques carried out by Research Group of MoMas, paper presented at 2nd International Meeting Clays in Natural and Engineering Barriers for Radioactive Waste Confinement, Agence Nat. Pour la Gestion des Dechets Radioactifs, Tours, France, 14–18 March.

Collin, F. (2003), Couplages thermo-hydro-mécaniques dans les sols et les roches tendres partiellement saturés, Ph.D. thesis, 300 pp., Univ. de Liege, Liege, Belgium.

Collin, F., R. Chambon, and R. Charlier (2006), A finite element method for poro mechanical modelling of geotechnical problems using local second gradient models, *Int. J. Numer. Methods Eng.*, *65*, 1749–1772, doi:10.1002/nme.1515.

Coussy, O. (1995), *Mechanics of Porous Continua*, John Wiley, London.

Delay, J., A. Vinsot, J. M. Krieguer, H. Rebours, and G. Armand (2007), Making of the underground scientific experimental programme at the Meuse/Haute-Marne underground research laboratory, north eastern France, *Phys. Chem. Earth*, *32*, 2–18.

Dracos, T. (1980), *Hydrologie, eine Einführung für Ingenieure*, Springer, Vienna.

Ewen, J., and H. R. Thomas (1989), Heating unsaturated medium sand, *Geotechnique*, *3*, 455–470.

Ghezzehei, T. A., R. C. Trautz, S. Finsterle, P. J. Cook, and C. F. Ahlers (2004), Modeling coupled evaporation and seepage in ventilated cavities, *Vadose Zone J.*, *3*, 806–818.

Hassanizadeh, M., and W. Gray (1979a), General conservation equations for multi-phase systems: 1. Average procedure, *Adv. Water Resour.*, *2*, 131–144, doi:10.1016/0309-1708(79)90025-3.

Hassanizadeh, M., and W. Gray (1979b), General conservation equations for multi-phase systems: 2. Mass, momenta, energy, and entropy equations, *Adv. Water Resour.*, *2*, 191–208, doi:10.1016/0309-1708(79)90035-6.

Hoxha, D., A. Giraud, A. Blaisonneau, F. Homand, and C. Chavant (2004), Poroplastic modelling of the excavation and ventilation of a deep cavity, *Int. J. Numer. Anal. Methods Geomech.*, *28*, 339–364, doi:10.1002/nag.346.

Kowalski, S. J. (1997), Moisture transport, thermodynamics, and boundary conditions in porous materials in presence of mechanical stresses, *Chem. Eng. Sci.*, *52*(7), 1141–1150, doi:10.1016/S0009-2509(96)00480-0.

Lewis, R. W., and B. A. Schrefler (2000), *The Finite Element Method in the Static and Dynamic Deformation and Consolidation of Porous Media*, John Wiley, New York.

Mayhew, Y. R., and G. F. C. Rogers (1976), *Thermodynamic and Transport Properties of Fluids*, 2nd ed., Blackwell, Oxford, U.K.

Neerdael, B., and J. P. Boyazis (1997), The Belgium underground research facility: Status on the demonstration issues for radioactive waste disposal in clay, *Nucl. Eng. Design*, *176*, 89–96, doi:10.1016/S0029-5493(96)01346-5.

Nuth, M., and L. Laloui (2008), Effective stress concept in unsaturated soils: Clarification and validation of a unified framework, *Int. J. Numer. Anal. Methods*, 771–801.

Rutqvist, J., D. Barr, R. Datta, A. Gens, A. Millard, S. Olivella, C.-F. Tsang, and Y. Tsang (2005), Coupled thermal-hydrological-mechanical analyses of the Yucca Mountain drift scale test-Comparison of field measurements to predictions of four different numerical models, *Int. J. Rock Mech. Min.*, *42*, 680–697, doi:10.1016/j.ijrmms.2005.03.008.

Simo, J. C., and R. L. Taylor (1985), Consistent tangent operators for rate-independent elasto-plasticity, *Comput. Methods Appl. Mech. Eng.*, *48*, 101–118, doi:10.1016/0045-7825(85)90070-2.

van Genuchten, M. T. (1984), A closed-form equation for predicting the hydraulic conductivity of unsaturated soils, *Soil Sci. Soc. Am. J.*, *44*, 892–898.

Zheng, H., H. C. Dai, and D. F. Liu (2008), A variational inequality formulation for unconfined seepage problems in porous media, *Appl. Math. Modell.*, in press.

Zhongxuan, L., L. Fengzhi, L. Yingxi, and L. Yi (2004), Effect of the environmental atmosphere on heat, water and gas transfer within hygroscopic fabrics, *J. Comput. Appl. Math.*, *163*, 199–210, doi:10.1016/j.cam.2003.08.065.

Zienkiewicz, O. C., and R. L. Taylor (2000), *The Finite Element Method*, 5th ed., Butterworth-Heinemann, Stoneham Mass.

R. Chambon, Laboratoire 3S, UJF, INPG, CNRS, F-38041 Grenoble CEDEX 9, France.

R. Charlier, F. Collin, and P. Gerard, Architecture, Géologie, Environnement et Constructions, Université de Liège, Chemin des Chevreuils 1, B-4000 Liège, Belgium. (f.collin@ulg.ac.be)